

Stiffness Model of a Die Spring

Merville K. Forrester

Thesis submitted to the Faculty of the
Virginia Polytechnic Institute & State University
In partial fulfillment of the requirements for the degree of

Master of Science
In
Mechanical Engineering

Dr. Reginald G. Mitchiner, Chairman
Dr. Charles E. Knight
Dr. A. Wicks

October 17, 2001
Blacksburg, Virginia

Keywords: Helical spring, lateral stiffness, axial stiffness, moment stiffness,
finite element analysis, rectangular cross-section

Stiffness Model of a Die Spring

Merville K. Forrester

(ABSTRACT)

The objective of this research is to determine the three-dimensional stiffness matrix of a rectangular cross-section helical coil compression spring. The stiffnesses of the spring are derived using strain energy methods and Castigliano's second theorem.

A theoretical model is developed and presented in order to describe the various steps undertaken to calculate the spring's stiffnesses. The resulting stiffnesses take into account the bending moments, the twisting moments, and the transverse shear forces. In addition, the spring's geometric form which includes the effects of pitch, curvature of wire and distortion due to normal and transverse forces are taken into consideration.

Similar methods utilizing Castigliano's second theorem and strain energy expressions were also used to derive equations for a circular cross-section spring. Their results are compared to the existing solutions and used to validate the equations derived for the rectangular cross-section helical coil compression spring.

A finite element model was generated using IDEAS (Integrated Design Engineering Analysis Software) and the stiffness matrix evaluated by applying a unit load along the spring's axis, then calculating the corresponding changes in deformation. The linear stiffness matrix is then obtained by solving the linear system of equations in changes of load and deformation. This stiffness matrix is a six by six matrix relating the load (three forces and three moments) to the deformations (three translations and three rotations). The natural frequencies and mode shapes of a mechanical system consisting of an Additional mass and the spring are also determined.

Finally, a comparison of the stiffnesses derived using the analytical methods and those obtained from the finite element analysis was made and the results presented.

Acknowledgments

I would like to thank my advisor Dr. R. G. Mitchiner for the support and guidance provided during the course of my research.

I would also like to express my thanks to Dr. C. E. Knight and Dr. A. Wicks for serving on my graduate committee and for providing valuable insight in this project.

Last, but not least, I would like to thank my parents, my wife (Quentisha) and all other family members (especially Tv, Esther and uncle Philmore) for their support and encouragement during my graduate studies.

Table of Contents

TABLE OF CONTENTS	IV
LIST OF FIGURES	V
LIST OF TABLES	VI
INTRODUCTION	1
1.0 PROJECT OVERVIEW	1
LITERATURE REVIEW	4
FINITE ELEMENT METHODS	8
3.1 MODEL DEVELOPMENT	8
3.2 STATIC ANALYSIS:	12
3.4 DYNAMICS ANALYSIS:.....	20
THEORETICAL DEVELOPMENT OF THE MODEL.....	23
4.1 VECTOR FORMULATION.....	25
EXPERIMENTAL TESTING	35
5.1 AXIAL STIFFNESS DETERMINATION.....	35
EVALUATION OF PARAMETERS	40
6.2 SYSTEM MASS AND INERTIA MATRIX	41
DISCUSSION OF RESULTS	43
7.1 CIRCULAR CROSS-SECTION	46
7.3 DEVELOPMENT OF STIFFNESS EQUATIONS	47
CONCLUSIONS AND RECOMMENDATIONS	57
APPENDIX A. EQUATIONS FOR STIFFNESS MATRIX ELEMENTS.....	59
APPENDIX B. MODE SHAPES (I-DEAS)	66
REFERENCES	72
VITA	73

List of Figures

Figure 1.1 A rectangular cross-section helical coil compression spring.....	2
Figure 1.2 Summary of analysis process	3
Figure 2.1 The spring element and its coordinate systems [4].....	4
Figure 2.2 Forces and moments acting on spring coil [5]	5
Figure 2.3 Mechanical system investigated by Belingardi [6]	6
Figure 3.1 Finite element model	9
Figure 3.2 Isometric view of the rectangular cross-section helical spring	10
Figure 3.3 Spring dimensions [11]	11
Figure 3.4 Beam element.....	12
Figure 3.5 Six degrees of freedom system.....	13
Figure 3.6 Distortion of spring section due to torque [5].....	15
Figure 3.7 Prandtl's membrane analogy [5].....	16
Figure 3.8 Maximum shear stress in a rectangular cross-section.....	16
Figure 3.9 Spring model of a single turn using solid tetrahedron elements.....	18
Figure 3.10 Shear stress distribution across beam's cross-section.....	19
Figure 3.11 Spring system.....	20
Figure 4.1 Analytical diagram	23
Figure 4.2 Spring cross-section and coordinates.....	23
Figure 4.3 Independent moments and forces	25
Figure 4.4 Vector formulation parameters	25
Figure 4.5 Loads acting on cross-section.....	33
Figure 5.1 Test systems	35
Figure 5.2 Texture Analyzer	36
Figure 5.3 Force vs. Displacement (specifications)	37
Figure 5.4 Force vs. displacement (Texture analyzer)	38
Figure 5.5 Load application result.....	39
Figure 6.1 Dimensions used in parameter evaluation	40
Figure 7.1 Symmetrical stiffness elements	43
Figure 7.2 Circular cross-section stiffness values	44
Figure 7.3 Frequency response function (I-DEAS).....	45
Figure 7.4 Differential element and applied loads [5].....	46
Figure 7.5 Curved section used in Bienzenzo's theorem.....	47
Figure 7.6 Moment stiffness [1]	52
Figure 7.7 Spring under combined lateral and axial loading [1].....	55
Figure 7.8 Chart for finding factor C_1 [1]	56
Figure B.1 Y-translation	66
Figure B.2 X-translation	67
Figure B.3 Z-bending	68
Figure B.4 Y-bending.....	69
Figure B.5 X-bending.....	70
Figure B.6 Z-translation	71

List of Tables

Table 3.1 Displacement values used to determine convergence	15
Table 3.2 Modes and Frequency (I-DEAS).....	22
Table 5.1 Test conditions used by the Texture analyzer	37
Table 5.2 Spring specifications.....	37
Table 7.1 Stiffness comparison.....	54

Chapter One

Introduction

1.0 Project Overview

The primary function of a mechanical spring is to store energy by deflections or distortions under an applied load. The spring can be considered as an elastic member that exhibits linear elastic properties provided that the material is not stressed beyond its elastic limit. In this investigation, a rectangular cross-section helical coil compression die spring was analyzed and is shown in Figure 1.1.

This spring's practical application can be found in brake controllers, where it is used to regain an equilibrium state once hydraulic pressure vanishes. The spring is required to have significantly large lateral stiffness to minimize lateral displacements.

The analysis is extended to the round wire cross-section spring and the correspondence of axial solutions to known axial stiffness equations is made. In contrast to the rectangular cross-section spring, extensive study has been done by Wahl [1] and others in the design of circular cross-section helical compression springs.

The dynamic system under investigation consists of a mass and helical coil compression spring that is fixed rigidly at the base and allowed to oscillate about the spring's three orthogonal axes x , y and z . This system can be considered a multiple-degree-of-freedom system that allows six-degrees-of-freedom (three translations and three rotations) about the spring's x , y and z axes. The objective of this study is to determine the three-dimensional stiffness matrix of the compression spring that is loaded by axial and shear forces and moments.

The stiffnesses of the spring are derived using strain energy methods and Castigliano's second theorem. The resulting stiffnesses take into account bending moments, axial loads, shear loads and transverse shear forces. In addition, the geometric effects of the spring's cross-section were taken into consideration. A model of the system was created using I-DEAS software, and static and dynamic analyses were performed. These analyses resulted in stiffness terms, natural frequencies and mode shapes. The completed stiffness matrix was developed using the flexibility method.

A review of available literature was done in the area of helical compression spring design and a brief summary is presented in Chapter 2.

The z axial stiffness of the spring was determined experimentally and compared to the manufacturer's design specifications. A diagram summarizing the procedure is shown in Figure 1.2.



Figure 1.1 A rectangular cross-section helical coil compression spring

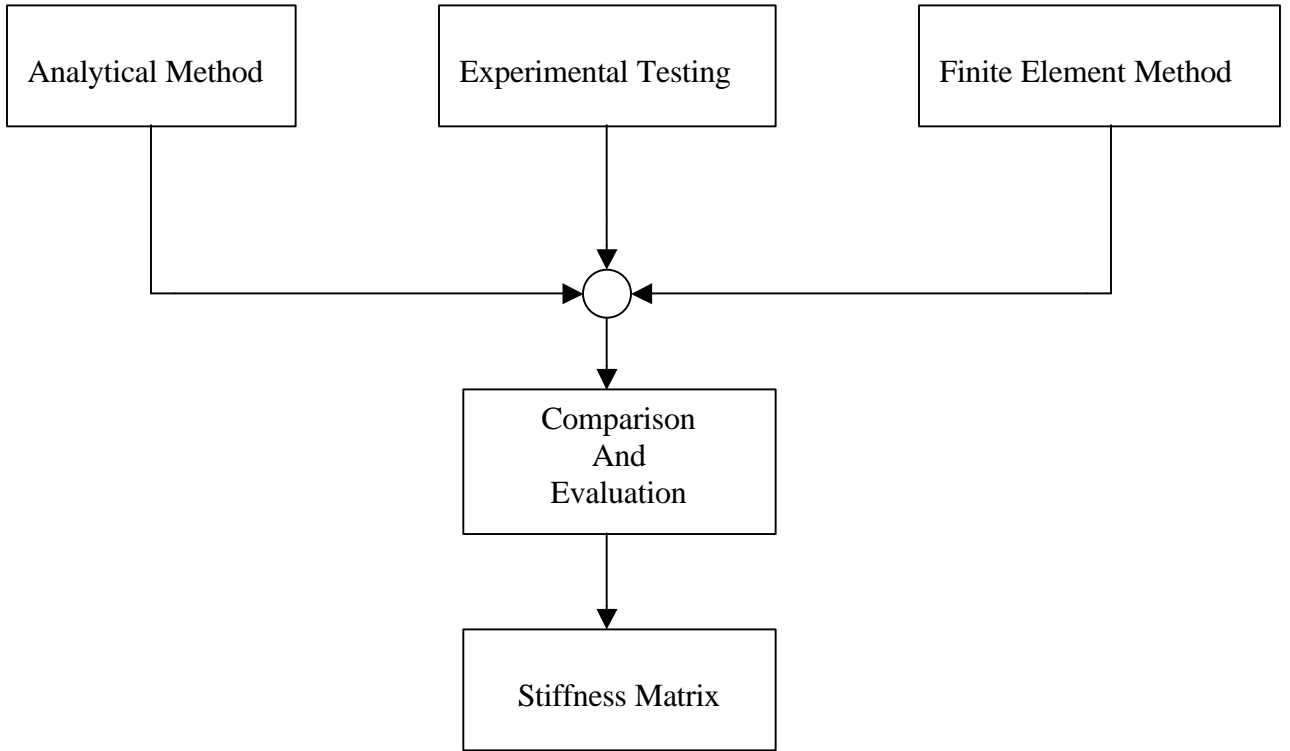


Figure 1.2 Summary of analysis process

Chapter Two Literature Review

In the analysis of a helical coil spring, one elementary model is often used, as by Haringx [2]. This model is comprised of a fictitious centerline that represents the coiled spring. However, effects of wire curvature, pitch and distortion due to loading conditions were neglected. Further study by Haringx was conducted for axially loaded springs. Additional investigations by Biezeno and Grammel [3] resulted in the local stiffness of a point along the centerline.

Lars Lindkvist [4] in his study, derived a model for the linear-deformation relationship for a small element of a coiled spring. Figure 2.1 shows the spring element used in his study.



Figure 2.1 The spring element and its coordinate systems [4]

This element was used to calculate the three-dimensional stiffness matrix of an arbitrary loaded coiled spring. The total spring was divided into small elements in which the deformation of each element was considered linear. Two coordinate systems were defined and used to describe the elements. The element under study was subjected to an arbitrary force $F = \{F_a, F_b, F_c\}$ and moment $M = \{M_a, M_b, M_c\}$ (which act along the a, b, c axes shown in Figure 2.1 above) at the center of the coil. Matrix formulation was used for load transformation from the global system to the local system. The elastic energy for a straight beam was written and Castigliano's theorem used to obtain the displacement of the spring element. The determination of the deformation resulted in elements of the stiffness matrix. Experimental testing was conducted using an oscillation spring and cube, lying on an adjustable surface. Various natural frequencies were calculated and compared at different tilting angles.

As described by Cook and Young [5], Castigliano's theorems are used to compute deflections. The helical spring is loaded by uni-axial forces or by a twisting moment and has a circular cross-section. Transverse shear deformation and direct stretching of the wire are considered negligibly small.

From Cook and Young and illustrated in Figure 2.2, the axial force F and twisting couple C are applied to the cross-section of the spring and are resolved into a bending moment M and a twisting moment T .

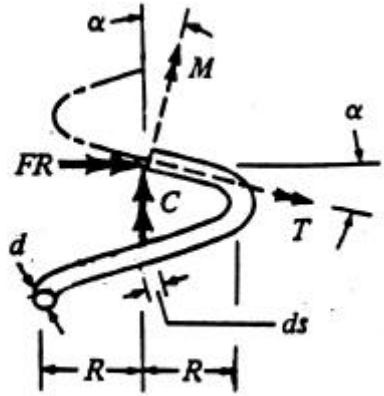


Figure 2.2 Forces and moments acting on spring coil [5]

The complementary strain energy was determined using Equation 2.1.

$$U^* = \int_0^L \left(\frac{M^2}{2EI} + \frac{T^2}{2GJ} \right) ds \quad (2.1)$$

Where

$$M = FR \sin \alpha + C \cos \alpha$$

$$T = FR \cos \alpha - C \sin \alpha$$

$$ds = \frac{Pd}{\cos \alpha}$$

$$E = 2G(1 + \nu)$$

$$J = \frac{\pi d^4}{32}$$

This relative extension Δ and rotation δ between ends of the helix are derived as follows:

$$\Delta = \frac{\partial U^*}{\partial F}$$

$$\Delta = \frac{\partial U^*}{\partial C} \quad (2.2)$$

From the above equations, the stiffness is easily determined using the linear-load relationship.

An additional solution to the lateral loading of a circular cross-section spring was presented by Belingardi [6]. The mechanical system investigated is shown in Figure 2.3.

- BC – coil spring
- AC – rigid beam
- A – point of rotation
- B, C – supports

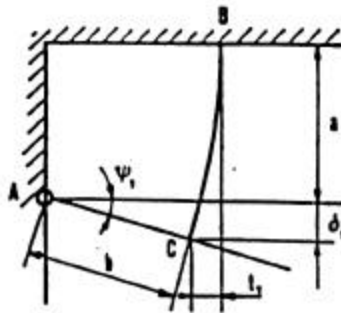


Figure 2.3 Mechanical system investigated by Belingardi [6]

The equations defining loads Q and M (not shown) acting at support C and the resulting torque T acting at B were derived. The resulting stiffness was determined by methods similar to those used by Cook and Young [5].

Belingardi [6] concluded that the resulting coefficients of lateral deflection and stiffness proved to show strong non-linearity relating the applied force to the lateral deflection. This becomes apparent for a given change in normal force. For a given lateral deflection, stresses were determined. The total stress in the spring is a combination of the stress due to the normal load and lateral deflection. The coefficients for lateral deflection, lateral stiffness and total stress were defined in a non-dimensionalized form to facilitate use in design.

This study focuses on the derivation of the three-dimensional stiffness matrix of a helical coil compression spring. The derivation takes into consideration the curvature of the spring, the shear effects and the geometry effects of the rectangular cross-section. An alternative approach to the matrix methods used by Lars Lindkvist [4] was implemented.

This formulation required vector analysis to define the coordinates and load components of the spring. When developing the stiffness, the spring was considered to be restrained such that each deflection of the ends of the spring occurred without deflections along any of the other five axes. Further, a lateral deflection of the top end of the spring must be resisted by a restoring moment in order to prevent rotation. All displacements are infinitesimal and the helix angle is not considered negligible.

Chapter Three

Finite Element Methods

In this study, the finite element analysis (FEA) was performed using I-DEAS® Master Series version 2.1 and 4.0, designed by the Structural Dynamics Research Corporation. Master Series is a comprehensive software package composed of a number of modules or applications, each of which is subdivided into “tasks”. The applications included in the software are, Design, Drafting, Simulation, Test, Manufacturing, Management and Geometry Translators.

Finite element analysis was applied to determine the stiffness and natural frequencies of the system. This method is based on the solution of differential equations with imposed boundary conditions. The system under investigation is an assembly of nodes that serve to connect elements together. The finite element model used is shown in Figure 3.1. For simplification, the model is shown displaying only nodes, restraints and beam elements as lines.

All elements used in I-DEAS have two defined sets of property tables; material and physical tables. Beam elements, however, have an additional cross section property which stores the entire geometrical description of the cross-section. In this analysis, solid rectangular beam cross-sections were used. Using the beam sections task of I-DEAS, properties such as moments of inertia and area are automatically computed from the section geometry.

Polynomial expressions are used to interpolate a given field quantity (displacement) over each element and therefore over the entire structure. It must be remembered that the finite element method is an approximate technique used to obtain a solution to a specific problem. The following procedure was used in obtaining the finite element solution:

- a) Generate a solid model of the spring.
- b) Create a grid of nodes connected by elements.
- c) Apply boundary conditions.
- d) Solving of static and dynamic models.
- e) Model updating.
- f) Display and interpreting of results.

3.1 Model Development

The geometry for the helical coil compression spring was modeled in the design application of I-DEAS [7]. The spring’s rendering was created from primitives (rectangles and circles) and the revolving of a 2-D section. An isometric view of the rectangular cross-section helical spring as modeled is shown in Figure 3.2. The resulting solid geometry was shared with the finite element analysis application.

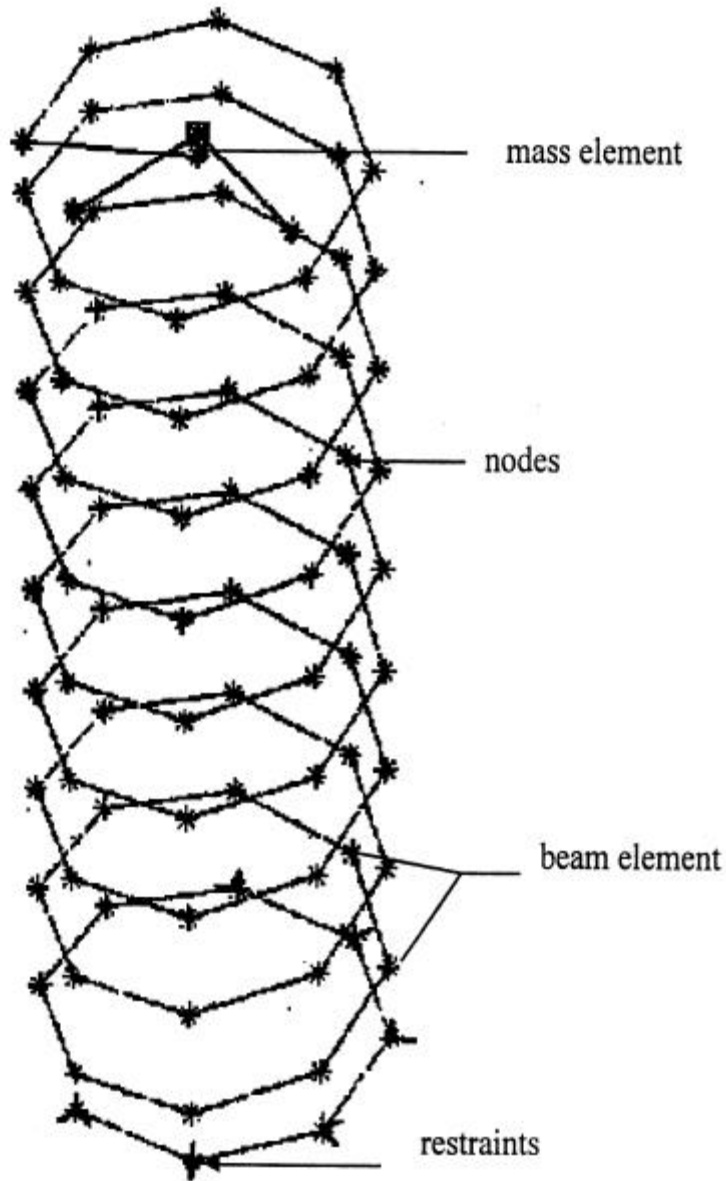


Figure 3.1 Finite element model

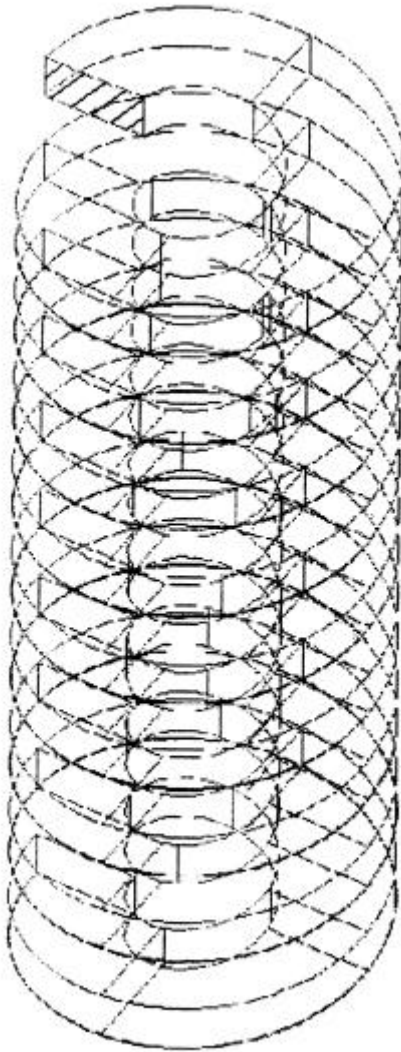


Figure 3.2 Isometric view of the rectangular cross-section helical spring

Solid representation of the part geometry provided the required information about the surfaces between the 3-D lines in space that is used to represent the spring. The solid geometry is a complete representation and therefore can be used to support the finite element analysis.

In order to insure accuracy in the modeled spring, a few finite element modeling guidelines were followed. First of all, various spring models with different number of elements per coil were generated and used as a standard for comparison (Table 3.1). The final model consisting of eight elements per coil, which also exhibited convergence of displacement values was used as the analysis model. For this model, the coil diameter was increased so that the combined length of the eight elements was equivalent to the circumference of the coil. This modification improved the material volume and mass.

The helical coil compression spring used throughout this investigation has the following specifications:



Figure 3.3 Spring dimensions [11]

Hole Diameter (O.D.): 0.75 in

Rod Diameter (I.D.): 0.375 in

Free height: 1.785 in

Rectangular wire size: 0.163 in (orthogonal to spring axis)
0.073 in (parallel to spring axis)

Pitch (free): 0.205 in

Total number of coils (N_t): 10

Number of active coils (N_a): 8

Both ends closed and ground.

Coil: Right hand

Material: Oil tempered wire, ASTM 229

$E = 207 \times 10^6 \text{ MPa} = 30.023 \times 10^6 \text{ psi}$

$G = 79.3 \times 10^6 \text{ MPa} = 11.50 \times 10^6 \text{ psi}$, $S_{ut} = 1400 \text{ MPa}$

Weight of spring, $w_{\text{spring}} = 0.0557 \text{ lb}$

Therefore

Mass of spring, $m_{\text{spring}} = w_{\text{spring}} / g$

$g = 386.34 \text{ in/s}^2$

$m_{\text{spring}} = 0.0001442 \text{ lbf.s}^2/\text{in}$

3.2 Static Analysis:

In the static modeling of the system, 1D linear beam elements were used to represent the helical coil compression spring. These elements mathematically modeled the overall deflection and bending moments of the spring. Their formulation is based on Timoshenko beam theory and includes transverse shear deformation. The actual helical compression spring can be approximated by a series of straight beams connected together. Two nodes are needed to define a beam element. The element's x axis connecting nodes one and two define the centroidal axis. The element y and z axes are the principal axes of the cross-section. To ensure correct orientation of the beam sections, the beam's cross-section geometry was displayed. A beam element used in the FE model is shown in Figure 3.4.

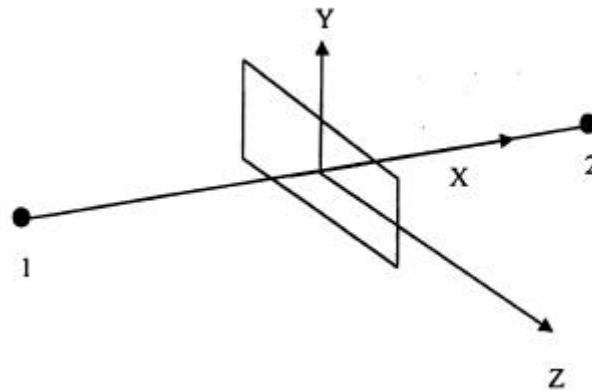


Figure 3.4 Beam element

There are six degrees of freedom (three translational degrees of freedom and three rotational degrees of freedom) assigned to each node.

At the base of the model, the nodes representing the inactive coil were completely restrained. This condition created the fixed base associated with the real system. The applied load was considered to be concentrated at the centerline of the spring and as a result, a rigid bar element was used to connect the beam element to a central node. The existence of the rigid bar element relates the motion of each node connecting the element to an infinitely rigid beam. Six degrees of freedom are assigned to each node. To represent the attached mass, a lumped mass element, which concentrates mass at a given node, was created at the central node. Originating from the central node were two perpendicular rigid elements, where forces and displacements were applied and computed respectively.

The elements of the stiffness matrix were determined based upon the linear load-deformation relationship

$$\{f\} = [k]\{x\} \quad (3.1)$$

As the spring is deformed, the spring exerts a force that is proportional to the displacement, but in an opposite direction. For this six degrees of freedom system, the resulting stiffness elements were determined by applying a single force and restraining all other degrees of freedom. The unit force applied at the position where displacements are defined determines respective elements of the stiffness matrix. Where moments of unit magnitude are applied, the corresponding rotations are maintained and all others set to zero.

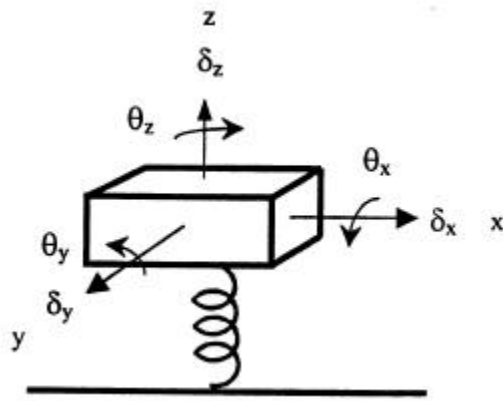


Figure 3.5 Six degrees of freedom system

For a unit force applied in the x direction, the corresponding stiffness element k_{xx} is mathematically determined as follows:

$$F_x = k_{xx}d_x + k_{xy}d_y + k_{xz}d_z + K_{xx}q_x + K_{xy}q_y + K_{xz}q_z \quad (3.2)$$

Static equilibrium position,

$$d_y = d_z = q_x = q_y = q_z = 0 \quad (3.3)$$

Stiffness,

$$k_{xx} = \frac{F_x}{d_x} \quad (3.4)$$

where k is the stiffness due to the applied force and K the stiffness due to the applied moments.

A similar procedure was carried out for forces and moments in x, y, z directions. The complete stiffness matrix is written as a 6 x 6 matrix and is shown symbolically in Equation 3.5.

$$[k] = \begin{bmatrix} k_{xx} & k_{xy} & k_{xz} & K_{xX} & K_{xY} & K_{xZ} \\ k_{yx} & k_{yy} & k_{yz} & K_{yX} & K_{yY} & K_{yZ} \\ k_{zx} & k_{zy} & k_{zz} & K_{zX} & K_{zY} & K_{zZ} \\ K_{Xx} & K_{Xy} & K_{Xz} & K_{XX} & K_{XY} & K_{XZ} \\ K_{Yx} & K_{Yy} & K_{Yz} & K_{YX} & K_{YY} & K_{YZ} \\ K_{Zx} & K_{Zy} & K_{Zz} & K_{ZX} & K_{ZY} & K_{ZZ} \end{bmatrix} \quad (3.5)$$

where

k – linear translational stiffness

K – rotational stiffness

x, y, z – translational directions

X, Y, Z – rotational directions

It should also be mentioned that the element stiffness matrix is symmetric.

The following stiffnesses were determined using the linear load-deformation relationship (explained above) and the FE model generated in IDEAS. These stiffnesses were evaluated based on the coordinate system defined in Figure 3.5 and this coordinate system will be used throughout the investigation.

$$[K] = \begin{bmatrix} 67.12 & 39.90 & 23.58 & 56.81 & 277.00 & 135.30 \\ 36.90 & 67.12 & 22.93 & 69.54 & 343.78 & 215.00 \\ 23.58 & 22.93 & 192.68 & 199.03 & 378.71 & 277.80 \\ 56.81 & 69.54 & 199.03 & 135.72 & 291.71 & 123.00 \\ 277.00 & 343.78 & 378.71 & 291.71 & 135.72 & 281.69 \\ 135.30 & 215.00 & 277.80 & 123.00 & 281.69 & 219.11 \end{bmatrix}$$

Convergence:

Obtaining an accurate final solution is very important in achieving reliable results. One sure way to accomplish this was to make additional models with increased number of beam elements per turn.

Z-displacements values were computed for a unit force applied in the z direction (compression) and these displacements were compared and checked for convergence. Table 3.1 shows the z-displacement values obtained.

Table 3.1 Displacement values used to determine convergence

Number of Beam Elements per coil	Maximum displacement in Z direction
4	5.1600061×10^{-3}
5	5.1800061×10^{-3}
6	5.1900060×10^{-3}
7	5.1900060×10^{-3}
8	5.1900061×10^{-3}

3.3 Torque loading on a Rectangular cross-section

The intent of this investigation is to accurately model the real spring using a finite element model. The spring experiences distortion along its cross-section similar to that depicted in Figure 3.6.

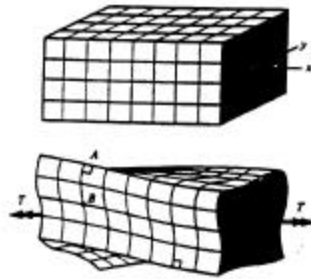


Figure 3.6 Distortion of spring section due to torque [5]

According to Saint-Venant's principle, a pure torque, constant along the length of the spring is applied as shear stresses that are distributed over the rectangular end cross-sections and throughout the spring's interior cross-sections. Shear stresses across a beam cross-section of the modeled spring were computed using I-DEAS and compared to Prandtl's membrane analogy relating to torsional stiffness. This analogy may be described as follows: A membrane is stretched over a flat rectangular plate and is subjected to a uniform tension at its edges. A uniform lateral pressure is applied which causes the membrane to bulge outwards (See Figure 3.7).

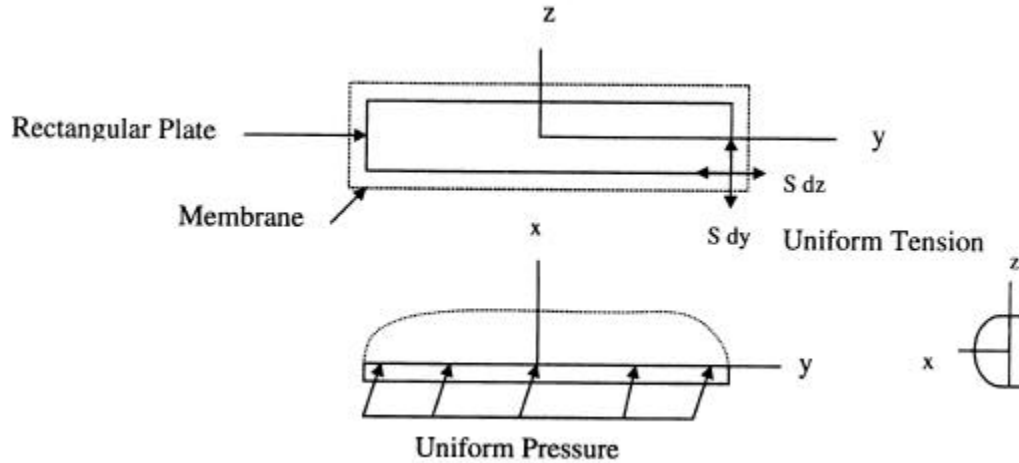


Figure 3.7 Prandtl's membrane analogy [5]

Further, the maximum slope of the membrane at any point represents the shearing stress at the corresponding point on the section.

Using I-DEAS, the computation of the shear stress involved a linear statics analysis test of one coil of the FE model shown in Figure 3.1. A torsional moment of unit magnitude was applied to the unrestrained end. The resulting shear stress distribution on the beam's cross-section is shown in Figure 3.10 as a contour display.

The maximum shear stress in a solid rectangular section loaded in torsion is located at A, (mid-points of long sides).

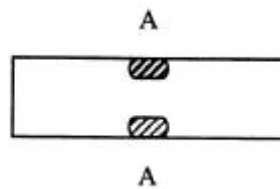


Figure 3.8 Maximum shear stress in a rectangular cross-section

By comparison, both IDEAS and Prandtl's membrane analogy resulted in similar maximum shear stress distributions. It is also worth mentioning that the shear stress is distributed according to Saint Venant's torsion theory for non-circular cross-sections.

Since strain energy methods were also used in the analytical solution, the resulting total strain energy was compared to the analytical solution. The FEM model shown in Figure 3.9 was created using solid parabolic tetrahedron elements.

The deformation of the coil that occurs when the initially unstressed coil is subjected to torsion stores work in the form of strain energy, U . A unit volume of a linear elastic material can be considered as a linear spring in which the load and displacement are linearly related. For this purpose, U and U^* (strain energy and complementary strain energy respectively) are numerically equal. As stated by Richards [11], the strain energy which varies along the spring is usually determined using the following:

Circular section

$$U = \frac{GJq^2}{2l} = \frac{1}{2}Tq = \frac{T^2l}{2GJ} = U^* \quad (3.6)$$

and for a non-circular section

$$U = \frac{GKq^2}{2l} = \frac{1}{2}Tq = \frac{T^2l}{2GK} = U^* \quad (3.7)$$

where

$$K = \frac{bt^3}{3}$$

Substituting the following into Equation 3.7

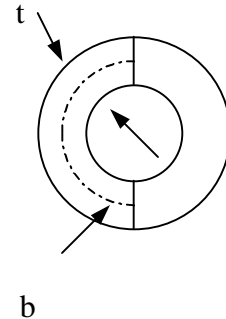
G = shear modulus = 11.50×10^6 psi

T = torque = 1lb.in

$b = 1$ = length of midline for one complete turn of spring = 1.6902 in

t = thickness = 0.163 in

K = torsional constant = 0.00244 in^4



The **total strain energy** is:

$U = 3.012 \times 10^{-5}$ in (**Analytical**)

$U = 3.371 \times 10^{-5}$ in (**I-DEAS**)

The preceding comparisons ensure the accuracy of IDEAS computations.

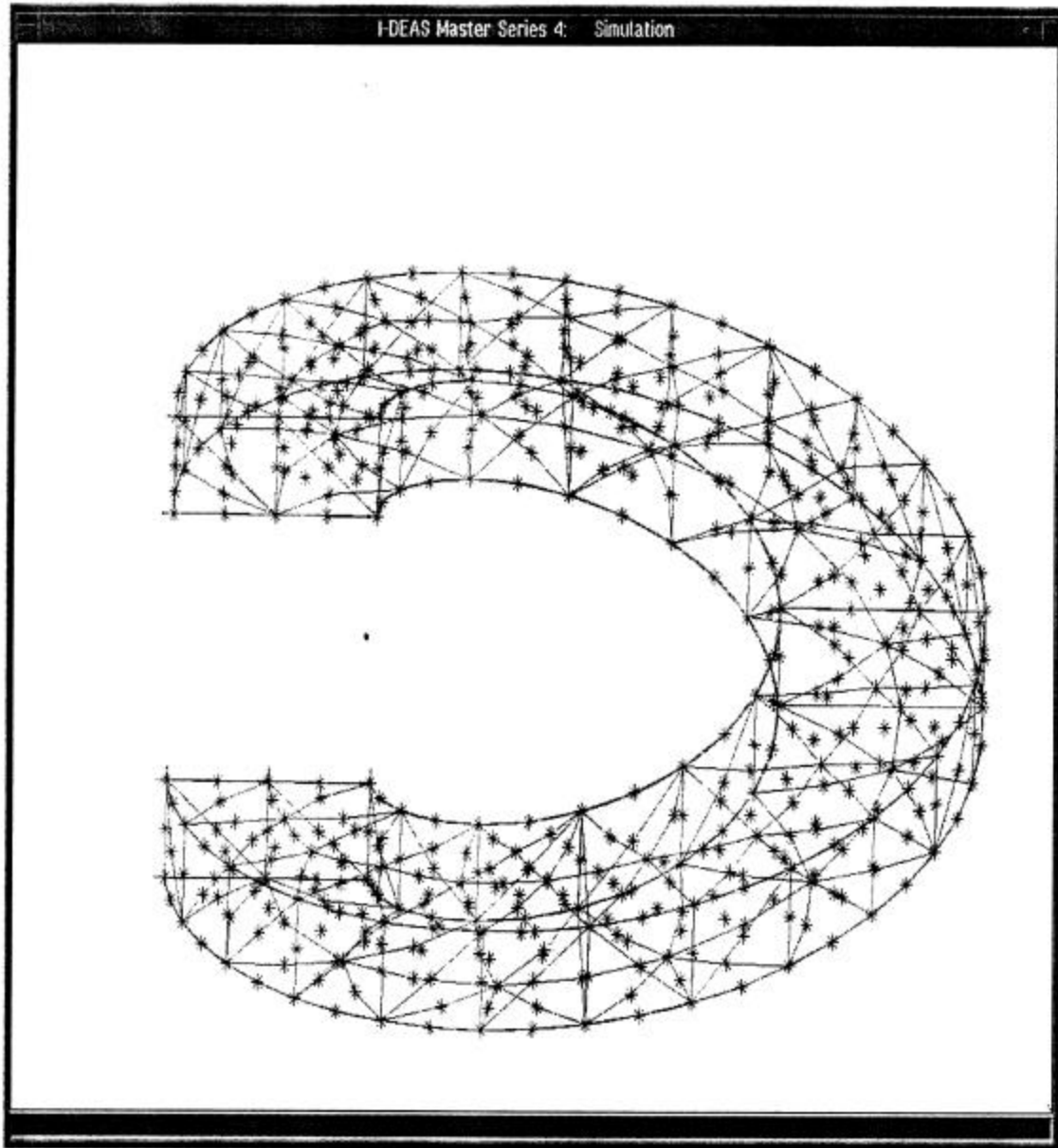


Figure 3.9 Spring model of a single turn using solid tetrahedron elements

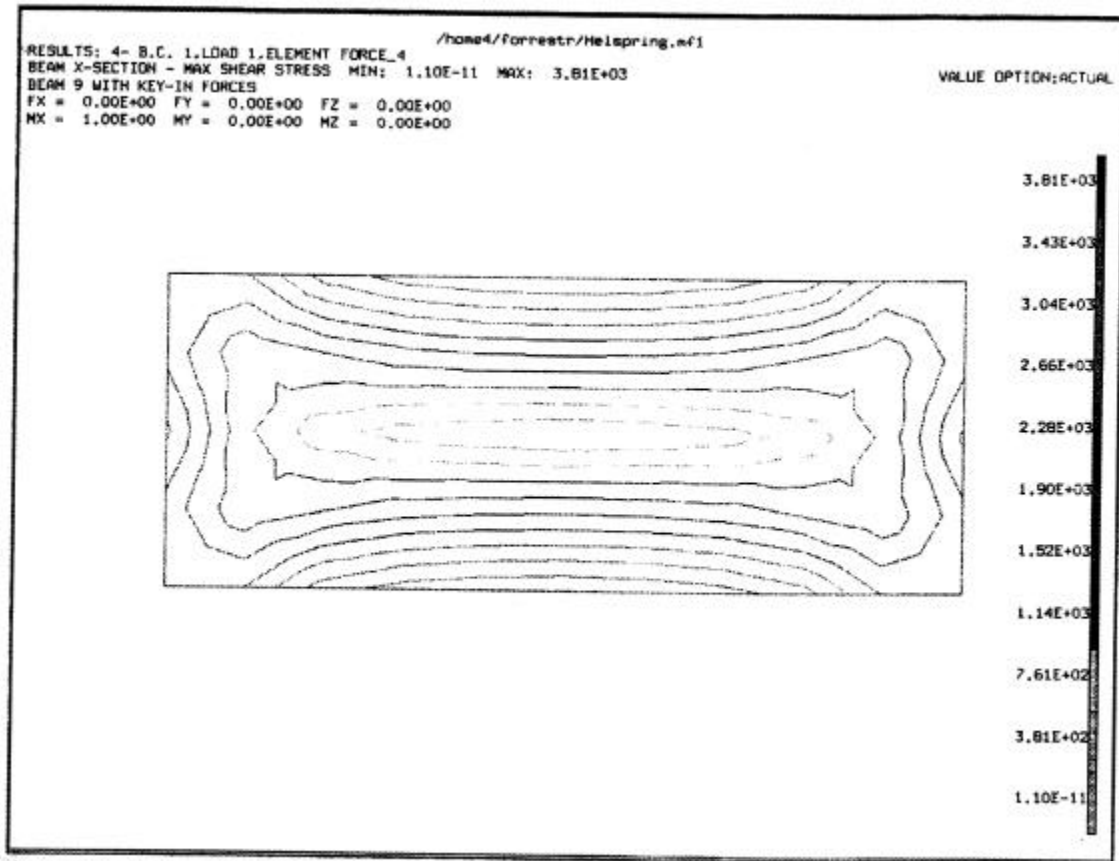


Figure 3.10 Shear stress distribution across beam's cross-section

3.4 Dynamics Analysis:

In this system, energy is transformed from kinetic energy to potential energy and back again. This results in a vibrating system. A vibrating system dissipates energy in the form of damping and the governing equation of motion representing this system is written in matrix form as:

$$[M]\{\ddot{X}\} + [C]\{\dot{X}\} + [K]\{X\} = \{F\} \quad (3.8)$$

where

$\{F\}$ – a vector force on each DOF in the system

$[M]$ – mass matrix

$[K]$ – stiffness matrix

$\{X\}, \{\dot{X}\}, \{\ddot{X}\}$ - displacement, velocity and acceleration of each DOF respectively
(physical DOF)

The I-DEAS software solves for the modes of vibration (natural frequencies and modes shapes) and uses these to calculate dynamic responses. The resulting equations of motion now contain diagonalized mass, stiffness and damping matrices which simplifies the mathematical calculations. In addition, the physical DOF's $\{X\}, \{\dot{X}\}, \{\ddot{X}\}$ are converted to modal degrees of freedom.

Using the Simulation application in IDEAS, the dynamic analysis was used to compute first the natural frequencies of the dynamic problem. The normal modes of vibration were solved using the SVI (Simultaneous Vector Iteration) method in the model solution task. Next, the equations of motion are solved to plot frequency responses to given inputs in the modal response task. This results in the frequency response function (FRF) graphs of given response points for a defined excitation function (see Figure 7.1). The viscous damping used in this analysis was obtained from experimental modal analysis methods.

To verify these results, an approximate value of the first natural frequency was calculated. The natural frequency of the system shown in Figure 3.11

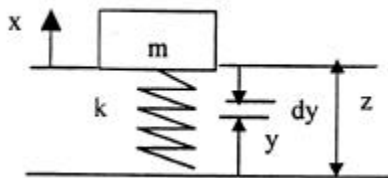


Figure 3.11 Spring system

Was determined using Rayleigh's method with effective mass [7]. Assuming that the velocity of an element in the spring, taken at a distance y from the fixed end varies linearly according to

$$\dot{x} \frac{y}{l} \tag{3.9}$$

where \dot{x} is the velocity of the lumped mass m .

The kinetic energy is generally written as:

$$T = \frac{1}{2} m_{eff} \dot{x}^2 \tag{3.10}$$

and for the spring:

$$\begin{aligned} T_{spring} &= \frac{1}{2} \int_0^L \left(\dot{x} \frac{y}{l} \right)^2 \frac{m_{spring}}{l} dy \\ &= \frac{1}{2} \frac{m_{spring}}{3} \dot{x}^2 \end{aligned} \tag{3.11}$$

The resulting effective mass is

$$\frac{m_{spring}}{3} \tag{3.12}$$

and the natural frequency used to verify the results is:

$$\omega_n = \sqrt{k / \left(m_{block} + \frac{m_{spring}}{3} \right)} \tag{3.13}$$

The primary interest of this method is to determine the natural frequency of vibration which is mainly a function of mass and stiffness of the system. The spring is considered massless and the system's mass is considered lumped.

Using the following:

Mass of Spring,	$m_{\text{spring}} = 0.0001442 \text{ lbf}\cdot\text{s}^2/\text{in}$
Mass of block,	$m_{\text{block}} = 0.005317 \text{ lbf}\cdot\text{s}^2/\text{in}$
Stiffness (I-DEAS),	$k = 192.678 \text{ lb/in}$ (Z axis)
Stiffness (Manufacturer specification),	$k = 190.10 \text{ lb/in}$

The natural frequencies computed using Equation 3.12 are:

I-DEAS	$\omega_n = 30.56 \text{ Hz}$ (Z-translation mode)
Experimental:	Manufacturer specifications, $\omega_n = 29.96 \text{ Hz}$

Table 3.2 Modes and Frequency (I-DEAS)

Modes	Frequency (Hz)
1 (y-translation)	5.813
2 (x-translation)	6.0346
3 (z-bending)	19.91
4 (y-bending)	20.292
5 (x-bending)	21.441
6 (z-translation)	30.556

Plots of the modes shapes obtained from I-DEAS are given in Appendix B.

Chapter Four Theoretical Development of the Model

In the analysis of the helical spring, vectorial methods were used in conjunction with Castigliano's second theorem to derive lateral, axial and moment stiffnesses. For simplification, the coiled spring can be represented as a centerline [Haringx]. Points along this line were described by a parametric vector $u(\hat{e})$, origination from the origin O of the orthogonal, normalized coordinate system i, j, k .

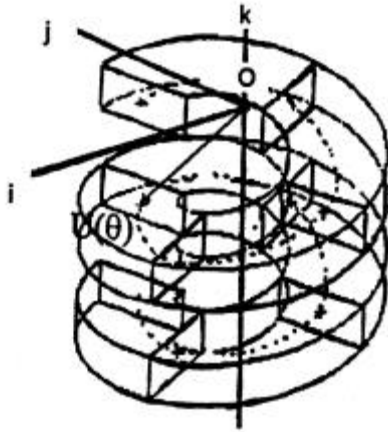


Figure 4.1 Analytical diagram

The applied lateral and axial loads were concentrated at the centerline of the spring, with a rigid structure imposed between the load application point and the start of the first active coil. The geometric effects of the rectangular cross-section were considered. Its cross-section was defined by orthogonal unit vectors s, t , and n . The spring's cross-section is shown below.

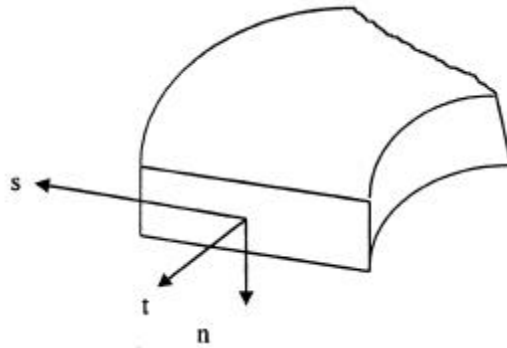


Figure 4.2 Spring cross-section and coordinates

Unit vector s is directed perpendicular to the spring axis and is parallel to the longest side of the cross-section. Unit vector t is directed axially through the cross-section and vector n is orthogonal to both s and t .

In determining the spring's stiffness, displacement (D_i) of the ends of the spring is considered to occur as the only component of the resultant displacement. To achieve this condition, the angular displacement due to the lateral load was resisted by a restoring moment (M_0) applied at the top end of the spring. Only the desired lateral displacement component is then obtained.

The complementary energy of the spring loaded by concentrated forces and moments is

$$\Pi^* = U^* - \sum_1^n P_i D_i \quad (4.1)$$

where P_i was used to define loads of unit magnitude comprising of either force F or moment M acting about the orthogonal axes (i, j, k) of the spring. For a force F acting along the x axis, $P_i = F_x i$ or in-terms of moments $P_i = F_x x i$.

Castigliano's second theorem is mathematically represented as

$$\frac{\partial U^*}{\partial P_i} = D_i \quad (4.2)$$

and yields the displacement component of the loaded point in the direction of the load. If load P includes forces F and moment M , the corresponding displacement D includes linear displacement Δ and angular displacement θ .

Equations 4.1 and 4.2 were used to determine these displacements. The complementary strain energy expression for a given length L is given as

$$U^* = \int_0^L \left(\frac{M_y^2}{2EI_y} + \frac{M_z^2}{2EI_z} + \frac{T^2}{2GJ} + \frac{N^2}{2EA} + k_y \frac{V_y^2}{2GA} + k_z \frac{V_z^2}{2GA} \right) dx \quad (4.3)$$

and was computed as the sum of the work done by six independent moments and forces (M_z, M_y, T, V_y, V_z, N) acting along the cross-section shown in Figure 4.2

In determining the stiffnesses across a section of the spring, vectorial methods were used. The following development describes the formulation of the stiffness expressions given the six independent forces and moments (M_z , M_y , T , V_y , V_z , N) acting in Figure 4.3.

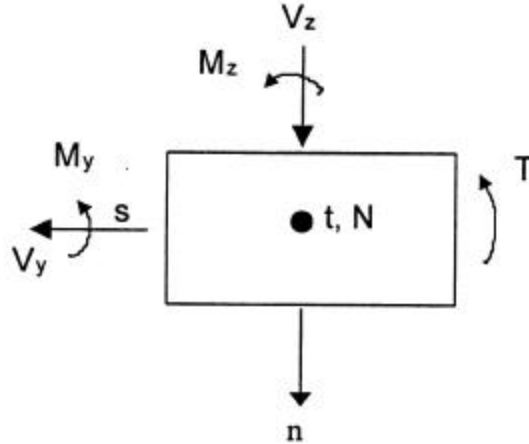


Figure 4.3 Independent moments and forces

4.1 Vector Formulation

Each point along the spring is defined by a position vector, \bar{u}

$$\bar{u} = \left(\frac{Pq}{2p} + x_o \right) \hat{i} + r \cos q \hat{j} + r \sin q \hat{k} \quad (4.4)$$

where

- P - pitch length
- x_o - offset
- r - spring radius
- \hat{e} - parameter

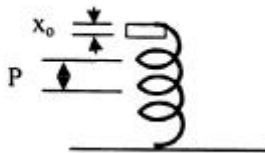


Figure 4.4 Vector formulation parameters

From which the following orthogonal unit vectors are derived:

$$\begin{aligned} \vec{t} &= \frac{d\vec{u}}{dq} \\ \vec{t} &= \frac{P}{2p} \hat{i} - r \sin q \hat{j} + r \cos q \hat{k} \end{aligned} \quad (4.5)$$

$$\vec{s} = r \cos q \hat{j} + r \sin q \hat{k} \quad (4.6)$$

$$\vec{n} = \vec{s} \times \vec{t}$$

$$\vec{n} = r^2 \hat{i} + \frac{Pr}{2p} \sin q \hat{j} - \frac{Pr}{2p} \cos q \hat{k} \quad (4.7)$$

The unit vectors s, t and n act as the origin through which the loads (forces and moments) are applied. The resulting normalized vectors were determined as follows:

$$\|\vec{s}\| = (r^2 \cos^2 q + r^2 \sin^2 q)^{\frac{1}{2}} \quad (4.8)$$

using the trigonometric identity

$$\cos^2 q + \sin^2 q = 1 \quad (4.9)$$

the norm of vector s is

$$\|\hat{s}\| = r$$

and the normalized vector calculated as

$$\hat{s} = \frac{\vec{s}}{\|\vec{s}\|} \quad (4.10)$$

results in

$$\hat{s} = \cos q \hat{j} + \sin q \hat{k}$$

A similar procedure was used for unit vectors t and n and resulted in the following normalized vectors:

$$\hat{t} = \frac{1}{\left(\sqrt{r^2 + \left(\frac{P}{2p}\right)^2}\right)} \left(\frac{P}{2p} \hat{i} - r \sin \hat{q} \hat{j} + r \cos \hat{q} \hat{k} \right) \quad (4.11)$$

$$\hat{n} = \frac{1}{\left(\sqrt{r^2 + \left(\frac{P}{2p}\right)^2}\right)} \left(r \hat{i} + \frac{P}{2p} \sin \hat{q} \hat{j} - \frac{P}{2p} \cos \hat{q} \hat{k} \right) \quad (4.12)$$

Since a position vector was defined for points along the spring, moment M_p , taken at an arbitrary point P (along the spring) was first defined in-terms of the global coordinates (i, j, k) then individual moments were taken along coordinates of interest (s, t, n).

Moment M_p ,

$$M_p = (-Lr \cos[\mathbf{q}] + Hr \sin[\mathbf{q}] + M_v) i + \left(\frac{LP\mathbf{q}}{2p} - rv \sin[\mathbf{q}] + M_L + Lx_o \right) j - \left(\frac{HP\mathbf{q}}{2p} - rv \cos[\mathbf{q}] + M_o - Hx_o \right) k \quad (4.13)$$

Initially, unit loads (H, V and L) were applied at the global origin O (Figure 4.1) and used in the derivations at point P along the spring.

Moment in the s direction is

$$M_{\hat{s}} = \vec{M}_p \cdot \hat{s} \quad (4.14)$$

which results in

$$M_{\hat{s}} = \frac{2p \cos[\mathbf{q}] M_L + 2p \sin[\mathbf{q}] M_o + (L \cos[\mathbf{q}] - H \sin[\mathbf{q}]) (P\mathbf{q} + 2px_o)}{2p}$$

To simplify the following expressions, an additional constant, c was defined

$$c = \sqrt{r^2 + \left(\frac{P}{2p}\right)^2} \quad (4.15)$$

Moment in the n direction

$$M\hat{n} = \vec{M}_p \cdot \hat{n} \quad (4.16)$$

$$M\hat{n} = \frac{1}{2p\sqrt{P^2 + 4p^2 r^2}} \left(\begin{array}{l} -2Pprv - 4LP^2 r^2 \text{Cos}[\mathbf{q}] + HP^2 \mathbf{q} \text{Cos}[\mathbf{q}] + 4HP^2 r^2 \text{Sin}[\mathbf{q}] + LP^2 \mathbf{q} \text{Sin}[\mathbf{q}] + \\ 2Pp\text{Sin}[\mathbf{q}]M_L - 2Pp\text{Cos}[\mathbf{q}]M_o + 4p^2 rM_v + 2HPP\text{Cos}[\mathbf{q}]x_o + 2LPp\text{Sin}[\mathbf{q}]x_o \end{array} \right)$$

where H and L are applied lateral forces along the y and x axes respectively and V is the applied axial force along the z axis.

The torque in the t direction

$$T = \vec{M}_p \cdot \hat{t} \quad (4.17)$$

$$T = \frac{1}{\sqrt{P^2 + 4p^2 r^2}} \left(\begin{array}{l} -LPr \text{Cos}[\mathbf{q}] + HPr \mathbf{q} \text{Cos}[\mathbf{q}] + 2pr^2 v \text{Cos}[2\mathbf{q}] + HPr \text{Sin}[\mathbf{q}] + \\ LPr \mathbf{q} \text{Sin}[\mathbf{q}] + 2pr\text{Sin}[\mathbf{q}]M_L + 2pr\text{Cos}[\mathbf{q}]M_o + PM_v - 2Hpr\text{Cos}[\mathbf{q}]x_o + 2Lpr\text{Sin}[\mathbf{q}]x_o \end{array} \right)$$

The axial force in the t direction is

$$N = \vec{v} \cdot \hat{t} + H \cdot \hat{t} \quad (4.18)$$

which when simplified results in

$$N = \frac{VP}{2pc} + \frac{Hr \sin \mathbf{q}}{c}$$

Similarly, the shear forces in the \vec{s} and \vec{n} directions are

$$\begin{aligned} Q\hat{s} &= \vec{v} \cdot \hat{s} + \vec{H} \cdot \hat{s} \\ &= H\text{Cos}\mathbf{q} \end{aligned} \quad (4.19)$$

and

$$Q\hat{n} = \frac{Vr}{c} + \frac{HP \sin \mathbf{q}}{2p}$$

In determining the restoring moment M_o that prevented rotation at the origin, the complementary strain energy

$$\frac{\partial U^*}{\partial M_o} = \mathbf{q}_o \quad (4.20)$$

was set to

$$\mathbf{q}_o = 0$$

and the moment M_o determined in terms of the lateral force (H) only. Mathematically this is represented as

$$\frac{\partial U^*}{\partial M_o} = \int_0^{16r} \left(\frac{M\hat{s}}{EI\hat{s}} \frac{\partial M\hat{s}}{\partial M_o} + \frac{M\hat{n}}{EI\hat{n}} \frac{\partial M\hat{n}}{\partial M_o} + \frac{T}{GJ} \frac{\partial T}{\partial M_o} + \frac{N}{EA} \frac{\partial N}{\partial M_o} + k\hat{s} \frac{Q\hat{s}}{GA} \frac{\partial Q\hat{s}}{\partial M_o} + k\hat{n} \frac{Q\hat{n}}{GA} \frac{\partial Q\hat{n}}{\partial M_o} \right) r d\mathbf{q} \cos \mathbf{y} \quad (4.21)$$

where

- ψ - the helix angle
- E - elastic modulus
- A - cross-sectional area
- G - shear modulus
- $I\hat{s}$ - area moment of inertia about s direction
- $I\hat{n}$ - area moment of inertia about n direction
- $k\hat{s}$ - shear factor for s direction
- $k\hat{n}$ - shear factor for n direction

For $V = 0$ and $L = 0$

$$\frac{\partial U^*}{\partial M_o} = \frac{r}{\cos \mathbf{y}} (I_1 + I_2 + I_3 + I_4 + I_5 + I_6) \quad (4.22)$$

where:

$$I_1 = \frac{1}{EI\hat{s}} \int_0^{16p} M\hat{s} \frac{\partial M\hat{s}}{\partial M_o} d\mathbf{q}$$

$$I_2 = \frac{1}{EI\hat{n}} \int_0^{16p} M\hat{n} \frac{\partial M\hat{n}}{\partial M_o} d\mathbf{q}$$

$$I_3 = \frac{1}{GJ} \int_0^{16p} T \frac{\partial T}{\partial M_o} d\mathbf{q}$$

$$\begin{aligned}
I_4 &= \frac{1}{EA} \int_0^{16p} N \frac{\partial N}{\partial M_o} d\mathbf{q} \\
I_5 &= \frac{k\hat{n}}{GA} \int_0^{16p} Q\hat{n} \frac{\partial M\hat{n}}{\partial M_o} d\mathbf{q} \\
I_6 &= \frac{k\hat{n}}{GA} \int_0^{16p} Q\hat{s} \frac{\partial Q\hat{s}}{\partial M_o} d\mathbf{q}
\end{aligned} \tag{4.23}$$

Evaluation of equation 4.22 results in an expression for the restoring moment

$$M_o = \frac{\frac{8HP^3}{c^2 p} + \frac{2HP^2 x_o}{c^2 p} + \frac{-32HPpr^2}{c^2} - \frac{8Hpr^2 x_o}{c^2} + \frac{1}{16p} \left(-2HPq^2 + HPCos[2q] - 2HPqSin[2q] - \right)}{\left(\frac{2P^2}{c^2 p} + \frac{8pr^2}{c^2 GJ} + \frac{8pq - 4pSin[2q]}{16p} \right)} \tag{4.24}$$

Using the Castigliano's second theorem, the displacement components of the loaded end of the spring are obtained as

$$\partial_H = \frac{\partial U^*}{\partial H} \quad \partial_L = \frac{\partial U^*}{\partial L} \quad \partial_V = \frac{\partial U^*}{\partial V} \tag{4.25}$$

and the angular displacement as

$$\mathbf{q}_H = \frac{\partial U^*}{\partial M_H} \quad \mathbf{q}_L = \frac{\partial U^*}{\partial M_L} \quad \mathbf{q}_V = \frac{\partial U^*}{\partial M_V} \tag{4.26}$$

Substituting these displacements into the linear load relationship (F=kx) and applying a unit load yields the following stiffness equations for the diagonal terms of the stiffness matrix (See Appendix A for the complete set of stiffness equations). In the following equations, the subscripts V, H and L are the stiffnesses along the z, y and x axes respectively.

Axial stiffness, k_v

$$k_v = \frac{(3AEGJ(P^2 + 4p^2 r^2)Cos[\mathbf{j}])}{\left(8r \left(6GJP^2 p v + 6AEGJP^2 pr^2 v + 12AEP^3 r^4 v + 24EJP^3 r^2 v k\hat{n} - 12AEGJP^2 R^2 V + \right) \right)} \tag{4.27}$$

Lateral stiffness, k_H (y axis)

$$k_H = \left(\frac{\text{Cos}[\mathbf{j}]}{\left(\frac{512P^4 \mathbf{p}}{3(P^2 + 4\mathbf{p}^2 r^2)} - \frac{8P^2 \mathbf{p} r^2}{P^2 + 4\mathbf{p}^2 r^2} + \frac{32\mathbf{p}^3 r^2}{P^2 + 4\mathbf{p}^2 r^2} + \frac{32\mathbf{p}^3 r^2}{AEP^2 + 4AEP^2 r^2} + \frac{P^4}{P^2 \mathbf{p} + 4\mathbf{p}^2 r^2} + \frac{8\mathbf{p} k \hat{s}}{AG} + \right.} \right. \\ \left. \left. r \left(\frac{8P^2 \mathbf{p} k \hat{n}}{P^2 + 4\mathbf{p}^2 r^2} - \frac{32P^3 \mathbf{p} M_o}{P^2 + 4\mathbf{p}^2 r^2} - \frac{64P^3 \mathbf{p} x_o}{P^2 + 4\mathbf{p}^2 r^2} - \frac{8P^2 \mathbf{p} M_o x_o}{P^2 + 4\mathbf{p}^2 r^2} + \frac{8P^2 \mathbf{p} x_o^2}{P^2 + 4\mathbf{p}^2 r^2} + \right. \right. \\ \left. \left. 4\mathbf{p} r^2 (15P^2 + 512P^2 \mathbf{p}^2 + 192P\mathbf{p}^2 x_o + 24\mathbf{p}^2 x_o^2 - 24\mathbf{p}^2 M_o (4P + x_o)) \right) \right) \\ \left(3GJ(P^2 + 4\mathbf{p}^2 r^2) \right) + \frac{1}{96\mathbf{p}^2} \left(\begin{aligned} & 4P^2 \mathbf{q}^3 - 6P^2 \mathbf{q} \text{Cos}[2\mathbf{q}] + 3P^2 \text{Sin}[2\mathbf{q}] - 6P^2 \mathbf{q}^2 \text{Sin}[2\mathbf{q}] + 24P\mathbf{p} \mathbf{q}^2 x_o - \\ & 12P\mathbf{p} \text{Cos}[2\mathbf{q}] x_o - 24P\mathbf{p} \mathbf{q} \text{Sin}[2\mathbf{q}] x_o + 48\mathbf{p}^2 \mathbf{q} x_o^2 - 24\mathbf{p}^2 \text{Sin}[2\mathbf{q}] x_o^2 + \\ & P \text{Sin}[2\mathbf{q}] + 4\mathbf{p} \text{Cos}[2\mathbf{q}] x_o + 6\mathbf{p} M_o \left(\begin{aligned} & -2P\mathbf{q}^2 + P \text{Cos}[2\mathbf{q}] + 2P\mathbf{q} \text{Sin}[2\mathbf{q}] - \\ & 8\mathbf{p} \mathbf{q} k_o + 4\mathbf{p} \text{Sin}[2\mathbf{q}] x_o \end{aligned} \right) \end{aligned} \right) \right) \quad (4.28)$$

Lateral stiffness, k_L (x axis)

$$k_L = \left(\frac{\text{Cos}[\mathbf{j}]}{\left(\frac{512P^4 \mathbf{p}}{3(P^2 + 4\mathbf{p}^2 r^2)} - \frac{8P^2 \mathbf{p} r^2}{P^2 + 4\mathbf{p}^2 r^2} + \frac{32\mathbf{p}^3 r^2}{P^2 + 4\mathbf{p}^2 r^2} + \frac{32\mathbf{p}^3 r^2}{AEP^2 + 4AEP^2 r^2} + \frac{P^4}{P^2 \mathbf{p} + 4\mathbf{p}^2 r^2} + \frac{8\mathbf{p} k \hat{i}}{AG} + \right.} \right. \\ \left. \left. r \left(\frac{8P^2 \mathbf{p} k \hat{n}}{P^2 + 4\mathbf{p}^2 r^2} - \frac{32P^3 \mathbf{p} M_L}{P^2 + 4\mathbf{p}^2 r^2} - \frac{64P^3 \mathbf{p} x_o}{P^2 + 4\mathbf{p}^2 r^2} - \frac{8P^2 \mathbf{p} M_L x_o}{P^2 + 4\mathbf{p}^2 r^2} + \frac{8P^2 \mathbf{p} x_o^2}{P^2 + 4\mathbf{p}^2 r^2} + \right. \right. \\ \left. \left. 4\mathbf{p} r^2 (15P^2 + 512P^2 \mathbf{p}^2 + 192P\mathbf{p}^2 x_o + 24\mathbf{p}^2 x_o^2 - 24\mathbf{p}^2 M_L (4P + x_o)) \right) \right) \\ \left(3GJ(P^2 + 4\mathbf{p}^2 r^2) \right) + \frac{1}{96\mathbf{p}^2} \left(\begin{aligned} & 4P^2 \mathbf{q}^3 - 6P^2 \mathbf{q} \text{Cos}[2\mathbf{q}] + 3P^2 \text{Sin}[2\mathbf{q}] - 6P^2 \mathbf{q}^2 \text{Sin}[2\mathbf{q}] + 24P\mathbf{p} \mathbf{q}^2 x_o - \\ & 12P\mathbf{p} \text{Cos}[2\mathbf{q}] x_o - 24P\mathbf{p} \mathbf{q} \text{Sin}[2\mathbf{q}] x_o + 48\mathbf{p}^2 \mathbf{q} x_o^2 - 24\mathbf{p}^2 \text{Sin}[2\mathbf{q}] x_o^2 + \\ & P \text{Sin}[2\mathbf{q}] + 4\mathbf{p} \text{Cos}[2\mathbf{q}] x_o + 6\mathbf{p} M_L \left(\begin{aligned} & -2P\mathbf{q}^2 + P \text{Cos}[2\mathbf{q}] + 2P\mathbf{q} \text{Sin}[2\mathbf{q}] - \\ & 8\mathbf{p} \mathbf{q} k_o + 4\mathbf{p} \text{Sin}[2\mathbf{q}] x_o \end{aligned} \right) \end{aligned} \right) \right) \quad (4.29)$$

Moment Stiffness, K_v

$$K_v = \frac{GJ(P^2 + 4p^2r^2)\text{Cos}[j]}{16pr(-Pr(L(P + GJP) + 2GJprv) + (P^2 + 4GJp^2r^2)M_v)} \quad (4.30)$$

Moment stiffness, K_H

$$K_H = \frac{\text{Cos}[j]}{r \left(\left(-\frac{32HP^3p}{P^2 + 4p^2r^2} + \frac{8P^2pM_o}{P^2 + 4p^2r^2} - \frac{8HP^2px_o}{P^2 + 4p^2r^2} + \frac{32p^2r^2(M_o - H(4P + x_o))}{P^2 + 4p^2r^2} + \frac{1}{16p} \right) \right.} \\ \left. \left(-4p(-2q + \text{Sin}[2q])M_o + H(P) - 2q^2 + \text{Cos}[2q] \right) + 2q\text{Sin}[2q] + 4p(-2q + \text{Sin}[2q] + \text{Sin}[2q])x_o \right)} \quad (4.31)$$

Moment stiffness, K_L

$$K_L = \frac{\text{Cos}[j]}{r \left(\left(\frac{32HP^3p}{P^2 + 4p^2r^2} + \frac{8P^2pM_L}{P^2 + 4p^2r^2} - \frac{8LP^2px_o}{P^2 + 4p^2r^2} + \frac{32p^2r^2(M_L - L(4P + x_o))}{P^2 + 4p^2r^2} + \frac{1}{16p} \right) \right.} \\ \left. \left(4p(-2q + \text{Sin}[2q])M_L + L(P) - 2q^2 + \text{Cos}[2q] \right) + 2q\text{Sin}[2q] + 4p(-2q + \text{Sin}[2q] + \text{Sin}[2q])x_o \right)} \quad (4.32)$$

Parameters used in evaluation of stiffnesses:

Loads:

$L = H = V = 1\text{ lbf}$ (forces)

$M_H = M_L = M_V = 1\text{ lb.in}$ (moments)

Pitch, $P = 0.205\text{ in}$

Spring radius, $r = 0.0815\text{ in}$

Off-set distance, $x_o = 0.073\text{ in}$

Constant, $c = 0.8779$

Parameter, $\delta = 6.473 = 0.113\text{ rad}$

$\text{Cos}[\delta] = 0.9284$

Cross-sectional area, $A = 0.0119 \text{ in}^2$
 Shear modulus of elasticity, $G = 11.50 \times 10^6 \text{ psi}$
 Modulus of elasticity, $E = 30.023 \times 10^6 \text{ psi}$

$k_{\hat{n}} = 1.20$
 $k_{\hat{s}} = 1.20$ [Wahl, pg. 231: Table 7.2.1]

Length of midline of cross-section, $b = 1.6902 \text{ in}$
 Thickness, $t = 0.163 \text{ in}$

$J_R = 2.551 \times 10^{-3} \text{ in}^4$ (non-circular)
 $J = 6.930 \times 10^{-5} \text{ in}^4$ (circular)

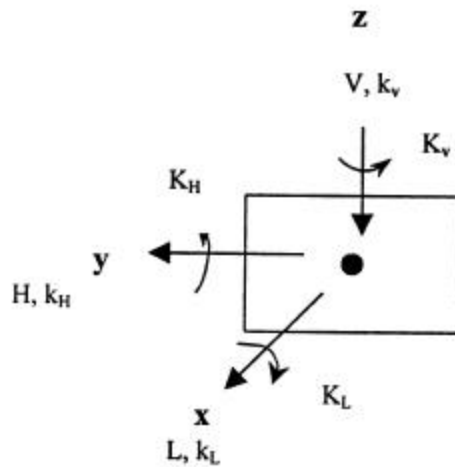


Figure 4.5 Loads acting on cross-section

Substitution of the stiffness parameters into Equations 4.27, 4.28, 4.29, 4.30, 4.31 and 4.32 results in the following stiffness values:

Lateral stiffness, $k_H = k_L = 69.32 \text{ lb/in}$ Moment Stiffness, $K_H = K_L = 119.40 \text{ lb-in/rad}$

Axial Stiffness, $k_v = 197.10 \text{ lb/in}$ Axial Moment stiffness, $K_v = 203.00 \text{ lb-in/rad}$

The calculation of the complete stiffness matrix involved obtaining solutions to equations resulting from the following matrix expression:

$$\left\{ \begin{array}{l} \mathbf{d}_H \\ \mathbf{d}_L \\ \mathbf{d}_V \\ \mathbf{q}_H \\ \mathbf{q}_L \\ \mathbf{q}_V \end{array} \right\} = \left[\begin{array}{cccccc} k_{xx} & k_{xy} & k_{xz} & K_{xX} & K_{xY} & K_{xZ} \\ k_{yx} & k_{yy} & k_{yz} & K_{yX} & K_{yY} & K_{yZ} \\ k_{zx} & k_{zy} & k_{zz} & K_{zX} & K_{zY} & K_{zZ} \\ K_{Xx} & K_{Xy} & K_{Xz} & K_{XX} & K_{XY} & K_{XZ} \\ K_{Yx} & K_{Yy} & K_{Yz} & K_{YX} & K_{YY} & K_{YZ} \\ K_{Zx} & K_{Zy} & K_{Zz} & K_{ZX} & K_{ZY} & K_{ZZ} \end{array} \right] \left\{ \begin{array}{l} H \\ L \\ V \\ M_H \\ M_L \\ M_V \end{array} \right\} \quad (4.33)$$

A complete listing of the equations for the individual stiffness elements is shown in Appendix A.

The following matrix contains the numerical values for the complete linear stiffness matrix derived analytically:

$$[K_{Analytical}] = \left[\begin{array}{cccccc} 69.32 & 48.00 & 36.30 & 65.10 & 292.00 & 143.00 \\ 48.00 & 69.32 & 37.11 & 81.50 & 356.20 & 235.00 \\ 36.30 & 37.11 & 197.10 & 219.00 & 391.00 & 300.00 \\ 65.10 & 81.50 & 219.00 & 119.40 & 319.00 & 141.00 \\ 292.00 & 356.20 & 391.00 & 319.00 & 119.40 & 270.00 \\ 143.00 & 235.00 & 141.00 & 141.00 & 270.00 & 203.00 \end{array} \right] \quad (4.34)$$

Chapter Five Experimental Testing

5.1 Axial stiffness determination

To check the validity of the calculations in the previous sections (specifically the stiffness in the z direction), an experiment was conducted to evaluate the k_{zz} stiffness term of the stiffness matrix. The arrangement of the experiment simply consists of a Texture analyzer shown in Figure 5.2, which was used to apply an incremental compressive load to the test systems shown.

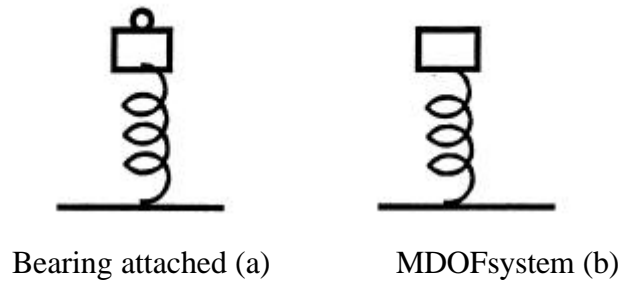


Figure 5.1 Test systems

System (a) consists of a bearing attached to a spring, whose base is rigidly fixed. This ensures that a normal load would be applied along the spring's axis (z-axis). System (b) is the actual multi-degree of freedom system under investigation and used here for comparison.

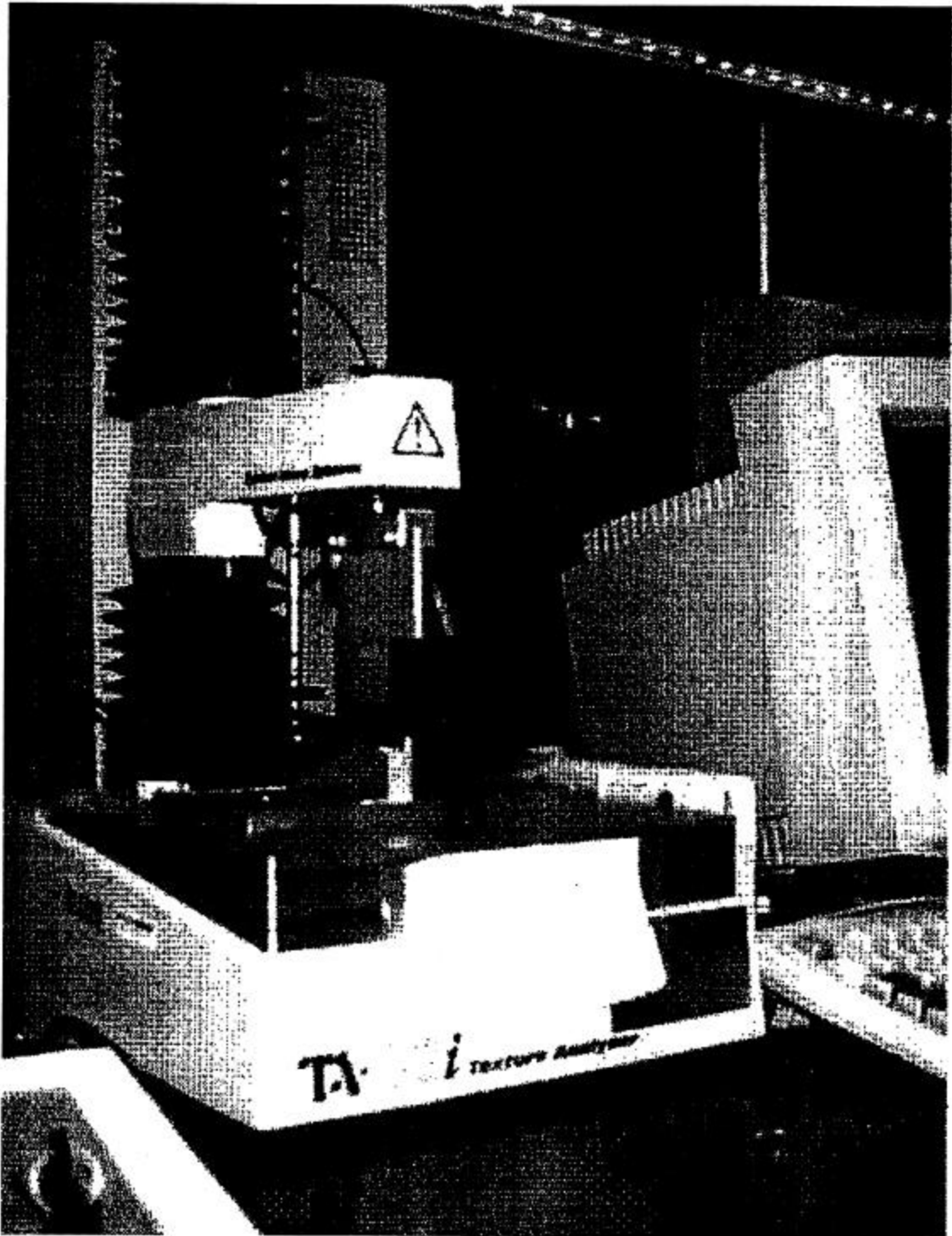


Figure 5.2 Texture Analyzer

The following table is a summary of the test conditions:

Table 5.1 Test conditions used by the Texture analyzer

Maximum force applied	220.65N
Minimum force applied	0 N
Maximum displacement	8 mm
Minimum displacement	0 mm
Force pre-speed	2.0 mm/s
Force post-speed	1.0 mm/s

A plot of force verses displacement generated by the Texture analyzer is given in Figure 5.4.

Using the manufacturers specifications, the z-axial stiffness was determined.

Spring's specifications:

Table 5.2 Spring specifications

Load at 50% deflection (0.8925 in)	Load at 1/10 deflection
154 lb	17.6 lb

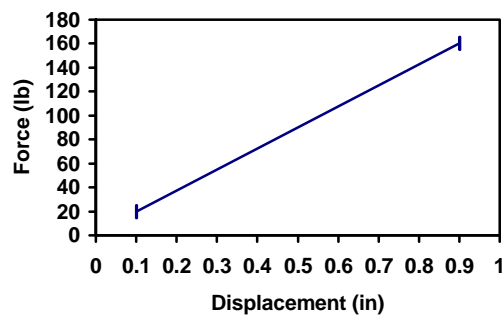


Figure 5.3 Force vs. Displacement (specifications)

Stable Micro Systems - Texture Expert

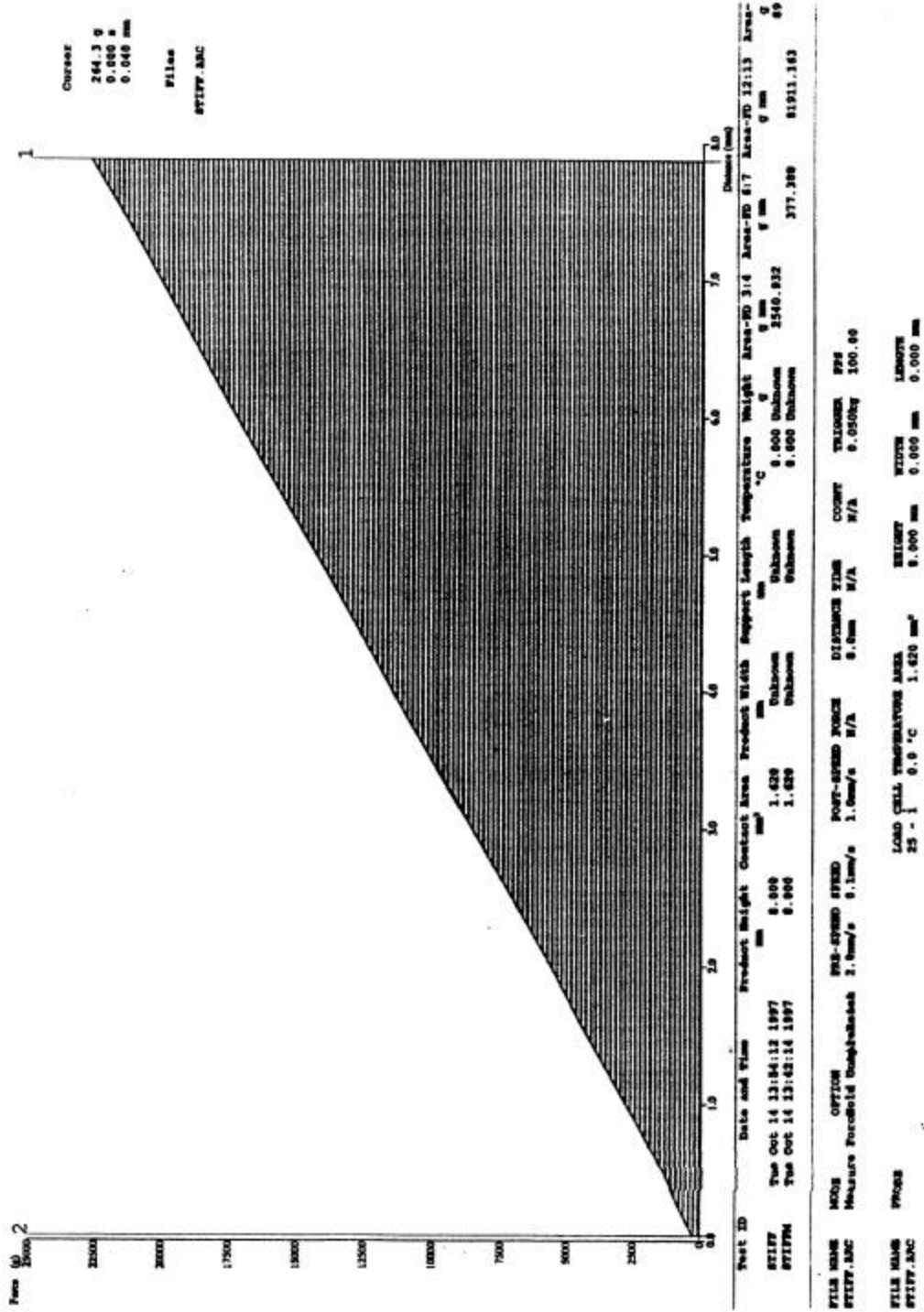


Figure 5.4 Force vs. displacement (Texture analyzer)

The axial stiffness is determined as:

$$k = \frac{\Delta f}{\Delta x} \quad (5.10)$$

Substituting:

$$\begin{aligned} f_2 &= 154 \text{ lb} & x_2 &= 0.8925 \text{ in} \\ f_1 &= 17.60 \text{ lb} & x_1 &= 0.175 \text{ in} \end{aligned}$$

into Equation (5.8), the axial stiffness is:

$$k_v = 190.10 \text{ lb/in}$$

It is interesting to note that the accuracy of the z-axial stiffness depends upon the point of application of the applied load. This conclusion was verified using the FE model in which a unit load was applied as an incremental ten percent offset from the springs z axis (see Figure 5.5 for load application results).

A plot of the incremental offset of the applied load verses the axial stiffness is illustrated below in Figure 5.5.

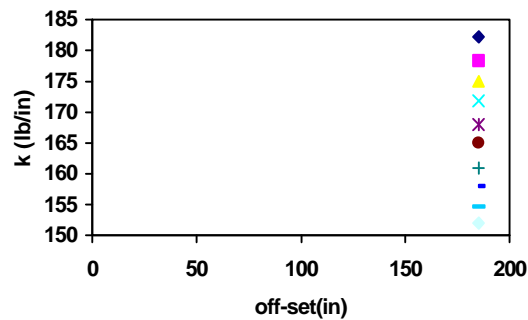


Figure 5.5 Load application result

A ten percent change in load application position results in approximately two percent difference in axial stiffness.

Chapter Six Evaluation of Parameters

6.1 System Properties:

Throughout the investigation, various properties were used and determined from calculations. The weight of the spring and block were measured using a balance and the inertia properties defined as follows:

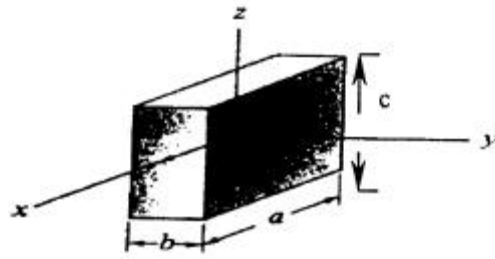


Figure 6.1 Dimensions used in parameter evaluation

Where $b = 1.75$ in
 $a = 2.375$ in
 $c = 1.75$ in

Material: steel, alloy
 $E = 30.023 \times 10^6$ psi
 $G = 11.50 \times 10^6$ psi
 $\tilde{\sigma} = 0.28$

Specific gravity = 7.8

weight density, = 0.28 lb/in^3

Mass of block, $m_{\text{block}} = 0.005317 \text{ lbf}\cdot\text{s}^2/\text{in}$

Free length, $L_o = 1.785$ in

Rectangular wire size, $t = 0.073$ in (parallel to spring axis)

$N_a = 8$

$$\text{Pitch of spring coils: } P = \frac{L_o - 2t}{N_a} = 0.205 \text{ in} \quad (6.1)$$

6.2 System Mass and Inertia matrix

The mass and inertial matrix emphasizes the inertial properties of the attached mass. For the system's mass,

$$M = \begin{bmatrix} M & 0 & 0 \\ 0 & M & 0 \\ 0 & 0 & M \end{bmatrix} \quad (6.2)$$

and mass inertia

$$I = \begin{bmatrix} I_{xx} & -I_{xy} & -I_{xz} \\ -I_{yx} & I_{yy} & -I_{yz} \\ -I_{zx} & -I_{zy} & I_{zz} \end{bmatrix} \quad (6.3)$$

Knowing that the mass moments of inertia about the x, y, and z axes passing through the mass center G of the mass is given as:

$$(I_{xx})_G = \frac{M}{12} (b^2 + c^2) = 2.7139 \times 10^{-3} \text{ lbf.in}^2$$

$$(I_{yy})_G = \frac{M}{12} (a^2 + c^2) = 3.8562 \times 10^{-3} \text{ lbf.in}^2$$

$$(I_{zz})_G = \frac{M}{12} (a^2 + b^2) = 3.8562 \times 10^{-3} \text{ lbf.in}^2$$

Since both of the orthogonal planes are planes of symmetry for the mass, the product of inertia with respect to these planes will be zero.

$$(I_{xy})_G = (I_{yz})_G = (I_{xz})_G = 0 \text{ lbf.in}^2$$

the mass moment of inertia about the base of the mass (where the spring is attached) is determined using the parallel axis theorem.

$$I_{xx} = (I_{xx})_G + m(y_G^2 + z_G^2) = 6.78473 \times 10^{-3} \text{ lbf.in}^2$$

$$I_{yy} = (I_{yy})_G + m(x_G^2 + z_G^2) = 7.9273 \times 10^{-3} \text{ lbf.in}^2$$

$$I_{zz} = (I_{zz})_G + m(x_G^2 + y_G^2) = 3.8562 \times 10^{-3} \text{ lbf.in}^2$$

$$I_{xy} = I_{yz} = I_{xz} = 0 \text{ lbf.in}^2$$

For the six degree of freedom system, the actual mass matrix is:

$$[M] = \begin{bmatrix} 0.005317 & 0 & 0 \\ 0 & 0.005317 & 0 \\ 0 & 0 & 0.005317 \end{bmatrix} \quad (6.4)$$

and the mass inertia matrix taken at the base of the attached mass is:

$$[I] = \begin{bmatrix} 0.0067847 & 0 & 0 \\ 0 & 0.0079273 & 0 \\ 0 & 0 & 0.0038562 \end{bmatrix} \quad (6.5)$$

Chapter Seven Discussion of Results

The work done due to the deformation of one coil of the spring is stored as strain energy. For a unit volume of the linear elastic spring, it was determined by comparison of results that the strain energy in the FE model adequately represented the strain energy determined analytically. For this reason, it can be assumed that the analytical assumptions are valid and were taken into consideration in I-DEAS calculations.

In determining the shear stresses across the rectangular cross-section, it is evident that the maximum shear stress is located at the midpoint of the long sides, as is suggested in Prandtl's membrane analogy. Equally important is the fact that under pure torsion circular and non-circular cross-sections behave differently. For the rectangular cross-section FE model (Figure 3.9), the coupled force used to apply pure torsion resulted in a warped cross-section. A similar load applied to a circular cross-section coil yielding no such effect.

The primary objective of this investigation was to derive expressions for the stiffness elements in the stiffness matrix for a rectangular cross-section spring. The resulting stiffness matrix is a symmetrical matrix containing 36 elements. A comparison between stiffnesses determined by analytical and finite element analysis methods is illustrated in the following figure. For simplification, only the symmetric stiffness terms are shown.

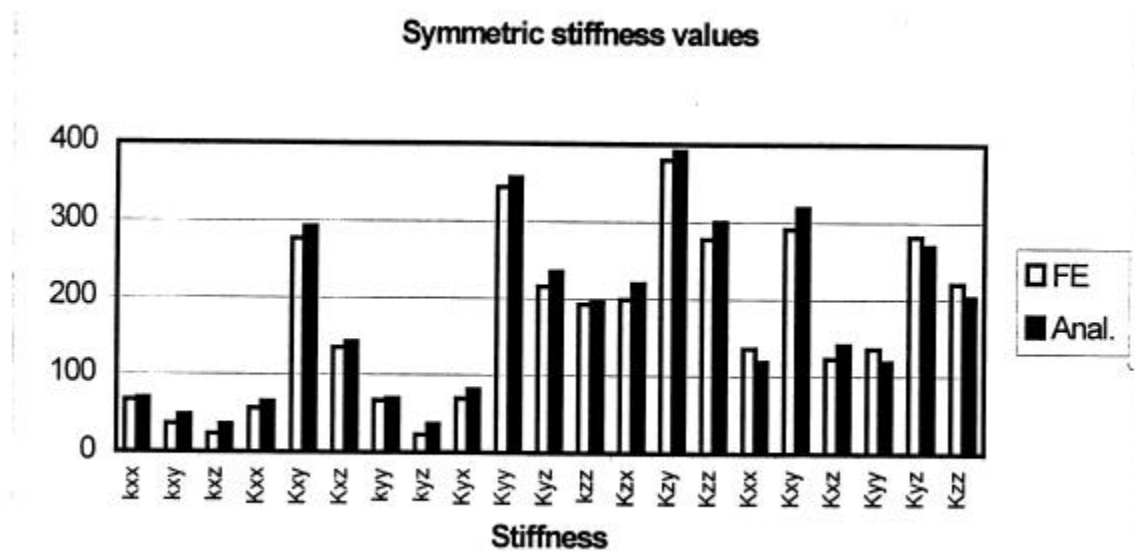


Figure 7.1 Symmetrical stiffness elements

In order to verify the accuracy of the equations derived for the stiffnesses in the rectangular cross-section, similar procedures were used to determine the expressions for a circular cross-section spring and their results compared to existing solutions. A comparative summary of the results is shown in Figure 7.2.

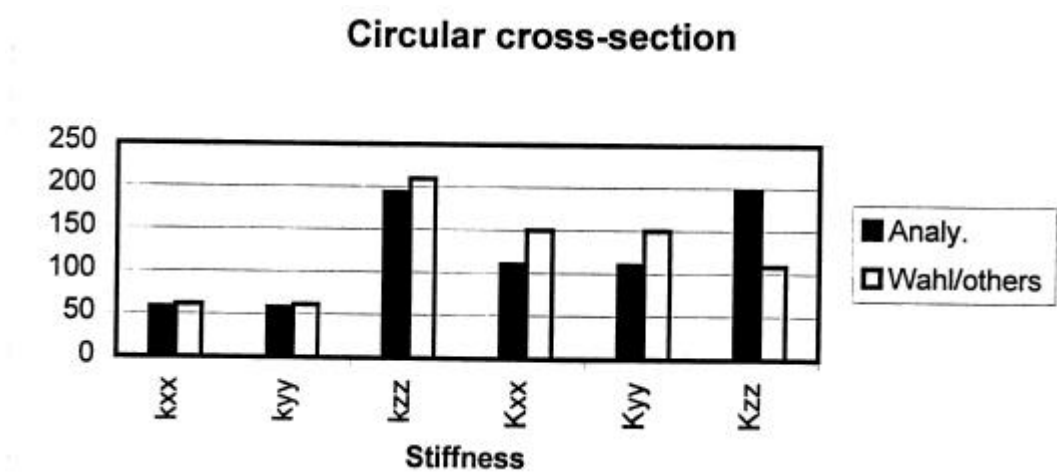


Figure 7.2 Circular cross-section stiffness values

The model response analysis task in I-DEAS displayed the frequency response function (FRF) of one input degree of freedom (DOF) location. An FRF is the ration of output to input taken at a given DOF, graphed verses frequency. The FRF was represented as magnitude and phase diagrams (Bode plots) on a logarithmic scale.

A graph oh the FRF function taken at the “driving point”, where the response was measured at the same point as the input (node 81-central node) and is shown in Figure 7.3.

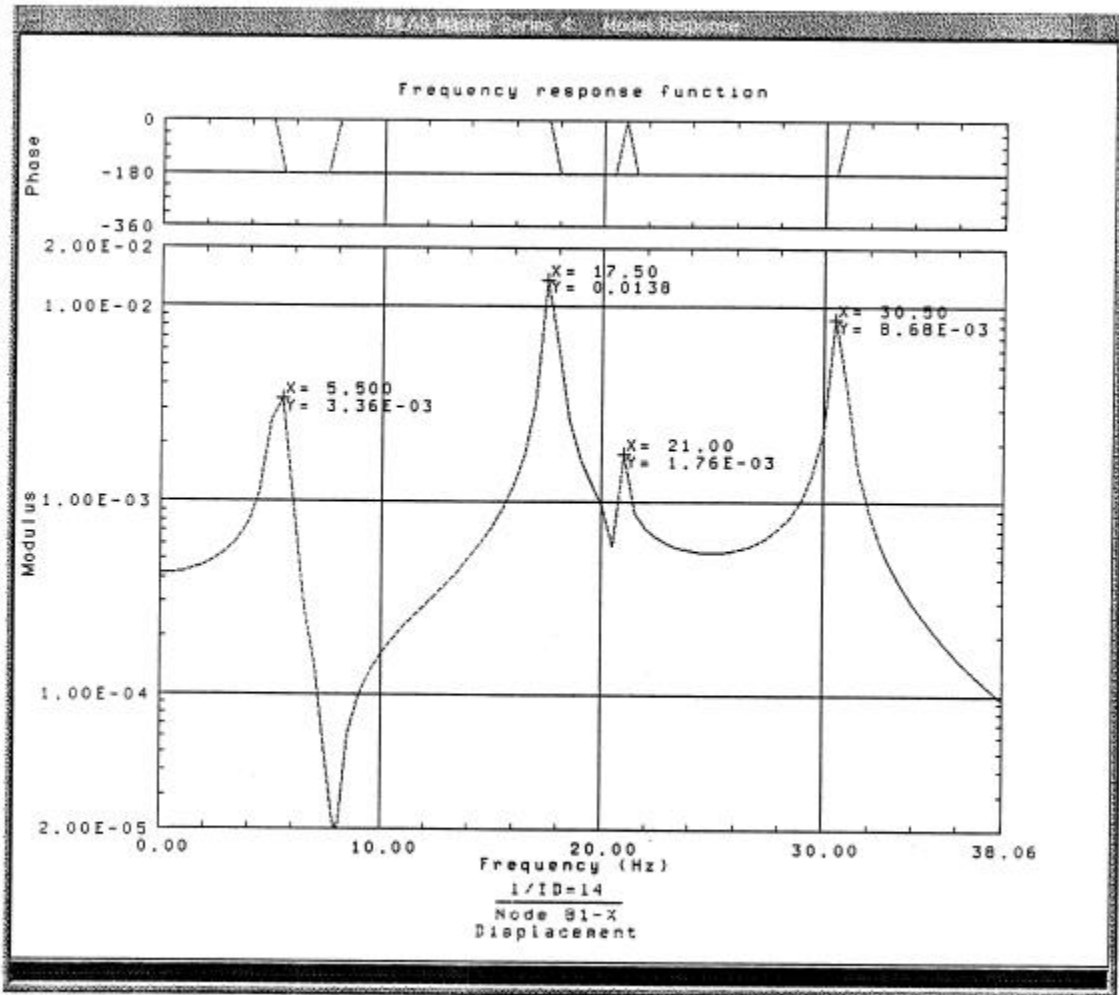


Figure 7.3 Frequency response function (I-DEAS)

7.1 Circular cross-section

This investigation primarily focuses on the analysis of rectangular cross-section helical coil compression springs. A similar analysis has been extended to circular cross-section helical coil springs and is discussed in the following section.

The analytical methods used were formulated in terms of vector quantities in which the applied forces, displacements and positions along the spring's helix are defined. As stated in section 3.2, the spring is considered linearly elastic and undergoes small deflections.

Static loads are applied to the spring and complementary energy methods and Castigliano's second theorem are used to compute deflections.

A volume element, dx , of the spring is considered with one end fixed.

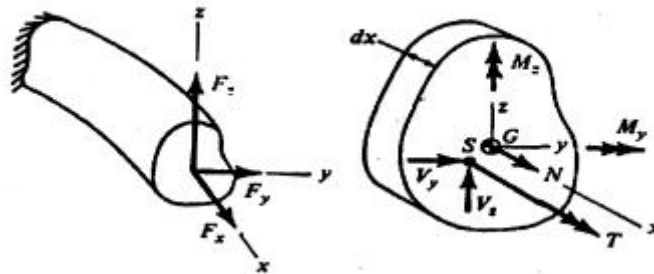


Figure 7.4 Differential element and applied loads [5]

The applied forces and moments at the free end causes displacement and rotations of the helix. Work is done by the applied forces and moments and is stored as strain energy. The strain energy is computed as the sum of the work done by the individual forces and moments as defined in section 4.0 using Equation 4.4.

In order to determine the properties used in the complementary strain energy expression (Equation 4.4), the following must be determined.

For a solid circular cross-section of radius r , the polar moment of inertia of the cross-section, J is

$$J = \frac{\pi r^4}{2} \quad (7.1)$$

Factors, $k_y = 1.11$ and $k_z = 1.11$, which account for the variation of transverse shear stress over the cross-section were obtained from table 7.21, Cook and Young [5].

The transverse shear force, bending moment and torque at an arbitrary point along the curved section of the spring can be determined using Biezenzo's theorem. Biezenzo's theorem states that at a given point A, on the section, the transverse shear force V, bending moment M, and torque T are

$$V_A = \sum_{i=1}^n P_i \quad (7.2)$$

$$M_A = \sum_{i=1}^n P_i R \sin f_i \quad (7.3)$$

$$T_A = \sum_{i=1}^n P_i R (1 - \cos f_i) \quad (7.4)$$

where

$$P_i - \text{reduced loads} = \frac{f_i F_i}{2p}$$

n – number of forces applied to the curved section

R – radius

f_i - angle from point of interest to ith normal force

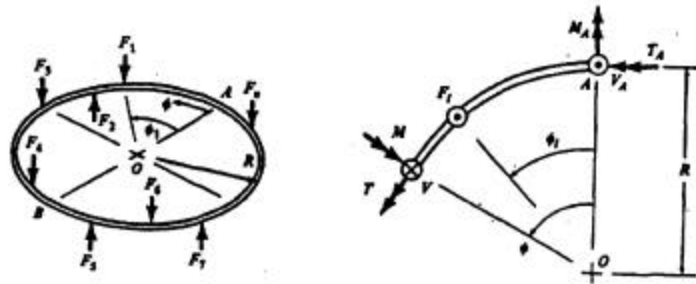


Figure 7.5 Curved section used in Biezenzo's theorem

7.3 Development of Stiffness equations

The theoretical development of the stiffness equations is discussed in the following section and parallels that used in Chapter four. Using vectorial methods, a parametric vector \bar{u} (è) was defined as:

$$\bar{u} = \left(\frac{Pq}{2p} + x_o \right) \hat{i} + r \cos q \hat{j} + r \sin q \hat{k} \quad (7.5)$$

The components of the externally applied lateral forces and restoring moments about orthogonal unit vectors s, t, n defining the spring's cross-section were determined.

The complimentary strain energy due to bending, torsion, axial forces and shear forces in conjunction with Castigliano's second theorem was used to determine the moments in terms of the lateral forces.

The complimentary strain energy and Castigliano's second theorem were again used to determine the lateral deflection of the spring due to the lateral forces. Specifically, the partial derivative of the complimentary strain energy with respect to the lateral force was found and set equal to the lateral deflection. The lateral stiffness was obtained by dividing the lateral force by the lateral deflection. The resulting stiffness equation was derived as:

$$k_H = \frac{\text{Cos}[\mathbf{j}]}{\left(\begin{array}{l} \left(\frac{512P^4\mathbf{p}}{3(P^2 + 4\mathbf{p}^2r^2)} - \frac{8P^2\mathbf{p}r^2}{P^2 + 4\mathbf{p}^2r^2} + \frac{32\mathbf{p}^3r^2}{P^2 + 4\mathbf{p}^2r^2} + \frac{32\mathbf{p}^3r^2}{AEP^2 + 4AEP^2r^2} + \frac{P^4}{P^2\mathbf{p} + 4\mathbf{p}^2r^2} + \frac{8\mathbf{p}k\hat{s}}{AG} + \right. \\ \left. r \left(\frac{8P^2\mathbf{p}k\hat{n}}{P^2 + 4\mathbf{p}^2r^2} - \frac{32P^3\mathbf{p}M_o}{P^2 + 4\mathbf{p}^2r^2} - \frac{64P^3\mathbf{p}x_o}{P^2 + 4\mathbf{p}^2r^2} - \frac{8P^2\mathbf{p}M_o x_o}{P^2 + 4\mathbf{p}^2r^2} + \frac{8P^2\mathbf{p}x_o^2}{P^2 + 4\mathbf{p}^2r^2} + \right. \right. \\ \left. \left. 4\mathbf{p}r^2(15P^2 + 512P^2\mathbf{p}^2 + 192P\mathbf{p}^2x_o + 24\mathbf{p}^2x_o^2 - 24\mathbf{p}^2M_o(4P + x_o)) \right) \right) \\ \left(3GJ(P^2 + 4\mathbf{p}^2r^2) \right) + \frac{1}{96\mathbf{p}^2} \left(\begin{array}{l} 4P^2\mathbf{q}^3 - 6P^2\mathbf{q}\text{Cos}[2\mathbf{q}] + 3P^2\text{Sin}[2\mathbf{q}] - 6P^2\mathbf{q}^2\text{Sin}[2\mathbf{q}] + 24P\mathbf{p}\mathbf{q}^2x_o - \\ 12P\mathbf{p}\text{Cos}[2\mathbf{q}]x_o - 24P\mathbf{p}\mathbf{q}\text{Sin}[2\mathbf{q}]x_o + 48\mathbf{p}^2\mathbf{q}x_o^2 - 24\mathbf{p}^2\text{Sin}[2\mathbf{q}]x_o^2 + \\ P\text{Sin}[2\mathbf{q}] + 4\mathbf{p}\text{Cos}[2\mathbf{q}]x_o + 6\mathbf{p}M_o \left(\begin{array}{l} -2P\mathbf{q}^2 + P\text{Cos}[2\mathbf{q}] + 2P\mathbf{q}\text{Sin}[2\mathbf{q}] - \\ 8\mathbf{p}\mathbf{q}k_o + 4\mathbf{p}\text{Sin}[2\mathbf{q}]x_o \end{array} \right) \end{array} \right) \right)$$

To determine the axial stiffness, components of the externally applied axial forces acting alone about the orthogonal unit vectors s, t, and n defining the spring's cross-section were determined. The complimentary strain energy (Equation 4.4) and Castigliano's second theorem were used to determine the axial deflection due to the axial force. The resulting axial stiffness was obtained by evaluating the following equation:

$$k_v = \frac{1}{d_v} \quad (7.5)$$

and was derived as:

$$k_v = \frac{(3AEGJ(P^2 + 4\mathbf{p}^2r^2)\text{Cos}[\mathbf{j}])}{\left(8r \left(\begin{array}{l} 6GJP^2\mathbf{p}v + 6AEGJP^2\mathbf{p}r^2v + 12AEP^3r^4v + 24EJ\mathbf{p}^3r^2vk\hat{n} - 12AEGJP^2R^2V + \end{array} \right) \right. \\ \left. \left(6AEP\mathbf{p}M_v(-2GJP\mathbf{p}r^2 + P^2 + 4GJ\mathbf{p}^2r^2) \right) \right)$$

A similar procedure was used to determine the moment stiffness and this procedure resulted in the following equation for the moment stiffness:

$$K_H = \frac{\cos[\mathbf{j}]}{\left(r \left(-\frac{32HP^3\mathbf{p}}{P^2 + 4\mathbf{p}^2r^2} + \frac{8P^2\mathbf{p}M_o}{P^2 + 4\mathbf{p}^2r^2} - \frac{8HP^2\mathbf{p}x_o}{P^2 + 4\mathbf{p}^2r^2} + \frac{32\mathbf{p}^2r^2(M_o - H(4P + x_o))}{P^2 + 4\mathbf{p}^2r^2} + \frac{1}{16\mathbf{p}} \right) \right)}$$

$$\left(-4\mathbf{p}(-2\mathbf{q} + \sin[2\mathbf{q}]M_o + H(P) - 2\mathbf{q}^2 + \cos[2\mathbf{q}]) + 2\mathbf{q}\sin[2\mathbf{q}] + 4\mathbf{p}(-2\mathbf{q} + \sin[2\mathbf{q}] + \sin[2\mathbf{q}])x_o \right)$$

Using the following parameters:

Loads:

L = H = V = 1 lbf (forces)
M_H = M_L = M_V = 1 lb.in (moments)
Constant, c = 0.8779
Parameter, è = 6.473 = 0.113 rad
Cos [è] = 0.9284
Shear modulus of elasticity, G = 11.50 x 10⁶ psi
Modulus of elasticity, E = 30.023 x 10⁶ psi

k_n = 1.20
k_s = 1.20 [Wahl, pg. 231: Table 7.2.1]

Spring specifications:

Rod Diameter (I.D.) = 0.375 in
Hole Diameter (O.D.) = 0.75 in
Pitch, P = 0.205 in
Spring radius, r = 0.0815 in
Off-set distance, x_o = 0.073 in
Cross-sectional area, A = 0.0119 in²
Thickness, t = 0.163 in
Free length: 1.785 in
Number of active coils (N_t) = 8
Coil: Right hand
Material: Oil tempered

-section, b = 1.6902 in

J = 6.930 x 10⁵ in (circular)

The stiffnesses were determined as:

Lateral stiffness H = k = 57.32 lb/in **Moment Stiffness** H = K = 110.13 lb-

, k_V 193.13 lb/in **Axial Moment stiffness, K** = 197.20 lb-

As stated, extensive work has been done by Wahl [5] and others and their analysis is used here to compare and justify the methods and results obtained in this investigation.

Axial stiffness:

Wahl [5] in his analysis stated that an element of an axially loaded helical spring of circular cross-section behaves essentially as a straight bar in pure torsion. The deflection of the spring will be:

$$\mathbf{d} = \frac{8PD^3n}{Gd^4} = 4.7767 \times 10^{-3} \text{ in [1]} \quad (7.6)$$

where

P = load. P = 1 lb

D = mean coil diameter, D = 0.5625 in

n = number of active coils, n = 8

d = bar diameter, d = 0.12 in

G = 11.50 x 10⁶ psi

From which the axial stiffness is determined as

$$\begin{aligned} k_v &= \frac{P}{\mathbf{d}_v} \\ &= 209.50 \text{ lb/in} \end{aligned} \quad (7.7)$$

Moment stiffness:

To calculate the deflection of a coiled spring subjected to moment in the plane of the axis of the spring (Figure 7.3a), Wahl [1] suggests considering a quarter coil subjected to a moment M at its end (Figure 7.3b). The moment being represented by a vector and at a cross-section at an angle, ϕ , the bending moment M_b , will be $M \cos \phi$ and the twisting moment, M_t will be $M \sin \phi$. For a given length $ds = r d\phi$ as shown in Figure 7.3 c, the component of the angular twist about the axis of the moment is given as:

$$d\mathbf{q} = \frac{M_b ds \cos \mathbf{j}}{EI} + \frac{M_t ds \sin \mathbf{j}}{GI_p} \quad (7.8)$$

where

ϕ = angular twist of a single coil of the spring

d = diameter of wire

n = number of active coils

M = moment in the plane of the spring

I, I_p = area and polar moment of inertia, $I_p = 2I$ (for circular cross-sections)

Further analysis by Wahl [1] defines the total angular twist, θ , for one complete turn as

$$\theta = \frac{Mr}{EI} \left(\frac{2G + E}{2G} \right)$$

p = torsional rigidity of the cross section
of the wire

Equation 7.9 is written as:

$$\theta = \frac{pMr}{EI} \left(\frac{2G + E}{2G} \right) \quad (7.10)$$

The moment stiffness in the lateral direction is then:

$$K = \frac{M}{\theta} + \frac{EI}{pr} \left(\frac{2G}{2G + E} \right) \quad (7.11)$$

given that M is the applied moment at the end of the spring coil.

Using the following:

$$r = D/2, r = 0.28125 \text{ in}$$

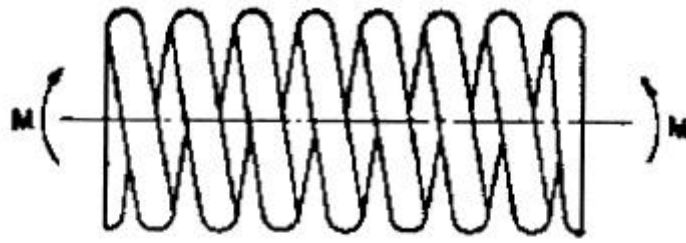
$$I = \frac{pd^4}{64} = 1.018 \times 10^{-5} \text{ in}^4$$

$$G = 11.50 \times 10^6 \text{ psi}$$

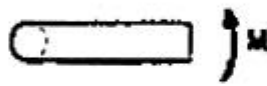
$$E = 30.023 \times 10^6 \text{ psi}$$

And from Equation 7.11, the **moment stiffness**,

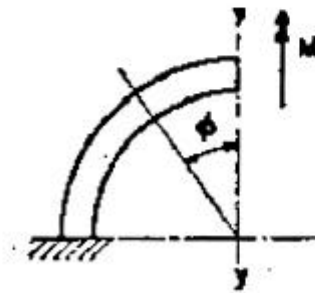
$$K_H = K_L = 150.045 \text{ lb-in/rad}$$



(a)



(b)



(c)

Figure 7.6 Moment stiffness [1]

Lateral stiffness:

A frequent application of helical springs is as vibration isolators, where they are laterally loaded by a force F while being compressed by a vertical force P . The only resistance to lateral deflection is the stiffness of the spring. Figure 7.4 illustrates this condition and the following theoretical analysis [Wahl] is used to determine the axial stiffness in the lateral direction.

For the given loading condition, Wahl states that the lateral stiffness is reduced by the presence of the axial load. The lateral stiffnesses determined by:

$$k_H = \frac{F}{d_x} = \frac{10^6 d^4}{C_1 n D (0.204 h_s^2 + 0.265 D^2)} \quad (7.12)$$

where

\ddot{a}_x = lateral deflection due to force F

D = mean coil diameter

d = bar diameter

h_s = compressed length of spring = $l_o - \ddot{a}_{st}$

\ddot{a}_{st} = vertical deflection due to load P

C_1 = factor depending on the ratio \ddot{a}_{st}/l_o and l_o/D

l_o = free length of the spring, $l_o = 1.785$ in

Values of C_1 may be taken from the chart shown in Figure 7.5.

The ratio of axial stiffness, $k_{zz} = P/\ddot{a}_{st}$ to lateral stiffness k_{xx} for a steel spring of round wire cross-section with $E = 30.023 \times 10^6$ psi and $G = 11.50 \times 10^6$ psi as derived by Wahl is

$$\frac{k_{zz}}{k_{xx}} = 1.44 C_1 \left(0.204 \frac{h_s^2}{D^2} + 0.265 \right) \quad (7.13)$$

$l_o = 1.785$ in

$\ddot{a}_{st} = 0.00519$ in (from IDEAS)

$h_s = l_o - \ddot{a}_{st} = 1.780$ in

$D = 0.5625$ in

$C_1 = 1.03$, $\ddot{a}_{st}/l_o = 0.00291$, $l_o/D = 3.173$

And substituting into Equation 7.12, **lateral stiffness**

$K_H = k_L = 61.27$ lb/in

From Equation 7.13, Axial stiffness, k_v

$$K_v = 209.72 \text{ lb/in}$$

Moment stiffness, K_v

In the analysis of a torsion spring, Shigley [15] determined the stiffness of one coil of a spring as:

$$K_v = \frac{d^4 E}{10Dn} \quad (7.14)$$

where

D = mean coil diameter = 0.5625 in

N = number of active coils = 8

d = bar diameter = 0.12 in

E = modulus of elasticity = 30.023×10^6 psi

Using Equation 7.14, the moment stiffness K_v

$$K_v = 138.34 \text{ lb.in/rad}$$

A summary of the stiffnesses is shown in Table 7.1 below and illustrated here for comparison.

Table 7.1 Stiffness comparison

Method	k_v	k_H	K_L	K_v	K_H	K_L
Analytical	193.13	57.32	57.32	197.2	110.13	110.13
Wahl	209.50	61.27	61.27	138.34	150.045	150.045

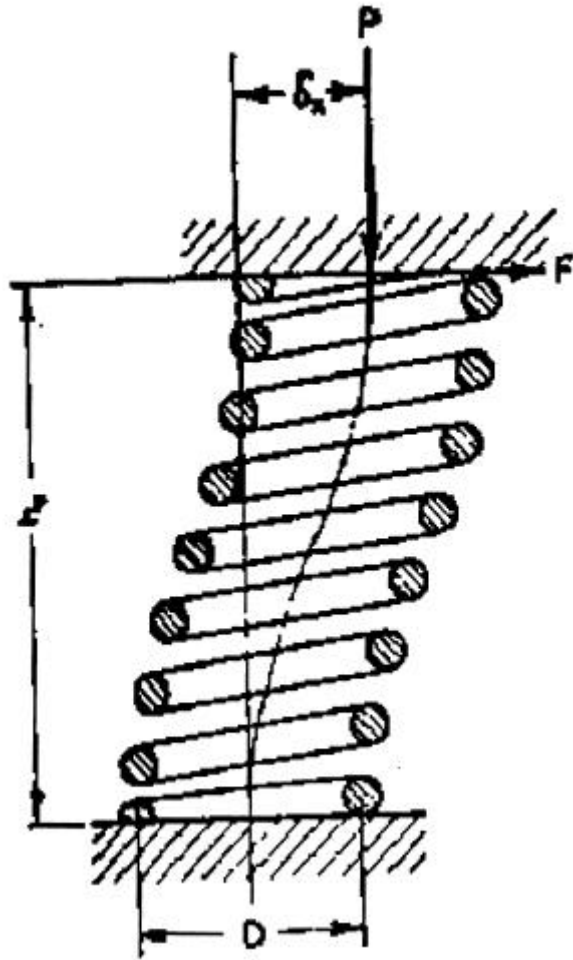


Figure 7.7 Spring under combined lateral and axial loading [1]

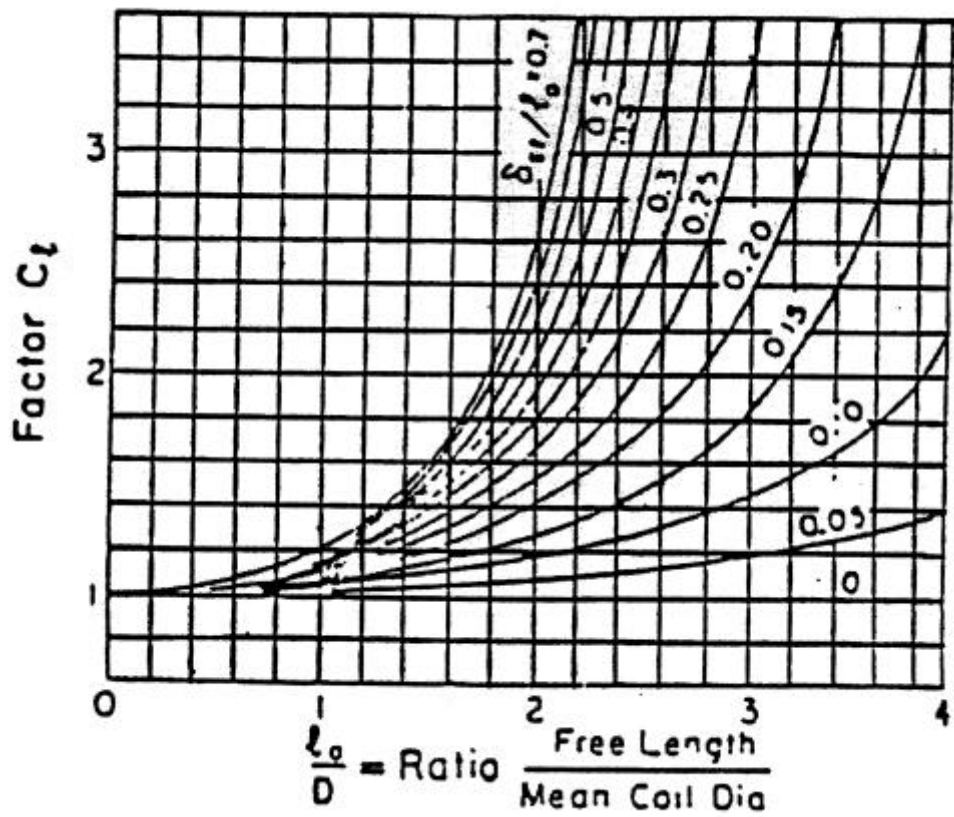


Figure 7.8 Chart for finding factor C_1 [1]

Chapter Eight

Conclusions and Recommendations

The primary objective of spring design is to obtain a spring which will be most economical for a given application and will have satisfactory life in service. Equally important is the spring's resistance to deformation under a given load.

In the preliminary investigation it was evident that extensive study has been done (Wahl [1] and others) in the design of circular cross-section springs, specifically in determining the stiffnesses due to various loading conditions. However, little analysis has been done for rectangular cross-section helical compression springs.

This investigation focused on determining the three-dimensional stiffness matrix for a rectangular cross-section helical compression spring and utilized Analytical methods, Finite element analysis and Experimental testing.

In the analytical analysis, the stiffness equations for axial, lateral and moment stiffness elements in the matrix were derived using Castigliano's second theorem and strain energy methods. The total stiffness matrix comprises of expressions derived for each element.

The FEA using I-DEAS which may be considered an "*ideal case scenario*", resulted in the stiffnesses, natural frequencies and mode shapes of the modeled spring. This was used in conjunction to experimental testing to verify the numerical results and equations derived.

To solve for the normal modes of vibration, the SVI (Simultaneous Vector Iteration) method was used. It is reported in I-DEAS Engineering Analysis User's Guide [12] that significant differences in natural frequencies may result from using other methods such as Guyan Reduction. In the future, the FE model may be solved using these methods and their solutions compared to the SVI solutions to see if the natural frequencies are significantly altered.

The analysis is also based on the linearity between load and deformation and the results of the analysis must be accepted subjected to the validity of this assumption. This assumption may be the primary cause of the erroneous data, specifically in the off diagonal terms of the stiffness matrix.

The finite element method is an approximate numerical technique for solving structural problems. It must also be remembered that inaccuracy may arise from the fact that the FE model is rarely an exact representation of the physical structure. The element mesh may not exactly fit the structure's geometry. In addition, the actual distribution of the load and possibly elastic properties may be approximated by simple interpolation functions. Boundary conditions simulating the rigid base may also be approximated.

If these factors are exactly represented, it is unlikely that the true displacement field can be exactly represented by the piecewise interpolation field permitted by a model having only a finite number of degrees of freedom.

As an additional verification procedure, similar analytical methods were used to derive equations for a circular cross-section helical coil compression spring and their numerical values compared to existing stiffness equations. Based on the comparison of the results, it is evident that correct formulation and procedures were implemented in deriving the stiffness equations for the rectangle cross-section spring. However, a fifteen-percent difference was determined and may have resulted due to explanations outlined in this chapter.

One important outcome worth noting is that the point of application of the load is important in determining the stiffness along the given axis. As shown in section 5.2, considerable error is induced if loads are applied offset to the spring's axis.

Further studies can also be done in the application of the stiffness equations to various configurations of mechanical systems. It may also be necessary to develop a computer based tool that may be used to predict the three dimensional stiffness of an arbitrarily loaded spring. Similar investigations may lead to the analysis of more complex cross-sections.

Finally, it must be remembered that even correctly computed results are developed from a conceptual model and not from reality itself thus may account for variations in results.

Appendix A. Equations for stiffness matrix elements

The total symbolic stiffness matrix and the equations for the individual elements are given in the following:

$$[k] = \begin{bmatrix} k_{xx} & k_{xy} & k_{xz} & K_{xX} & K_{xY} & K_{xZ} \\ k_{yx} & k_{yy} & k_{yz} & K_{yX} & K_{yY} & K_{yZ} \\ k_{zx} & k_{zy} & k_{zz} & K_{zX} & K_{zY} & K_{zZ} \\ K_{Xx} & K_{Xy} & K_{Xz} & K_{XX} & K_{XY} & K_{XZ} \\ K_{Yx} & K_{Yy} & K_{Yz} & K_{YX} & K_{YY} & K_{YZ} \\ K_{Zx} & K_{Zy} & K_{Zz} & K_{ZX} & K_{ZY} & K_{ZZ} \end{bmatrix} \quad (A.1)$$

where

k – linear translational stiffness

K – rotational stiffness

x, y, z – translational directions

X, Y, Z – rotational directions

$$k_{11} = \frac{\text{Cos}[j]}{\left(\frac{512P^4p}{3(P^2 + 4p^2r^2)} - \frac{8P^2pr^2}{P^2 + 4p^2r^2} + \frac{32p^3r^2}{P^2 + 4p^2r^2} + \frac{32p^3r^2}{AEP^2 + 4AEP^2r^2} + \frac{P^4}{P^2p + 4p^2r^2} + \frac{8pk\hat{t}}{AG} + \right. \\ \left. r \frac{8P^2pk\hat{n}}{P^2 + 4p^2r^2} - \frac{32P^3pM_o}{P^2 + 4p^2r^2} - \frac{64P^3px_o}{P^2 + 4p^2r^2} - \frac{8P^2pM_o x_o}{P^2 + 4p^2r^2} + \frac{8P^2px_o^2}{P^2 + 4p^2r^2} + \right. \\ \left. 4pr^2(15P^2 + 512P^2p^2 + 192Pp^2x_o + 24p^2x_o^2 - 24p^2M_o(4P + x_o)) \right) \\ \left(3GJ(P^2 + 4p^2r^2) + \frac{1}{96p^2} \begin{pmatrix} 4P^2q^3 - 6P^2q\text{Cos}[2q] + 3P^2\text{Sin}[2q] - 6P^2q^2\text{Sin}[2q] + 24Ppq^2x_o - \\ 12Pp\text{Cos}[2q]x_o - 24Ppq\text{Sin}[2q]x_o + 48p^2qx_o^2 - 24p^2\text{Sin}[2q]x_o^2 + \\ P\text{Sin}[2q] + 4p\text{Cos}[2q]x_o + 6pM_o \left(\begin{matrix} -2Pq^2 + P\text{Cos}[2q] + 2Pq\text{Sin}[2q] - \\ 8pqk_o + 4p\text{Sin}[2q]x_o \end{matrix} \right) \end{pmatrix} \right) \right) \quad (A.2)$$

$$k_{12} = \frac{r\text{Sin}^3q(\text{Cos}j - \text{Cos}^2qj - \text{Sin}^2q + \text{Sin}^2(2q))}{EA} + \frac{r^3\text{Sin}^3q(\text{Sin}^2j - \text{Sin}q + \text{Sin}^2(2q))}{\text{Cos}^2qEI} + \\ \frac{r^3\text{Sin}q\text{Sin}(j - q)}{GP} + \frac{\text{Sin}qr\text{Cos}j}{k\hat{s}GA} \quad (A.3)$$

$$k_{13} = \frac{r\sin^3\theta(\cos^2\theta\sin\varphi + \sin^2\theta\cos(2\theta) + \sin^2\theta\sin\varphi - \sin^2\theta\cos\varphi)}{EA} + \frac{r^3\sin^3\theta(\cos^2\theta\sin\varphi + \sin^2\theta)}{\cos^2\theta EI} + \frac{r^3\sin\theta\sin(\varphi - \theta)}{GP} - \frac{\sin\theta r\sin\varphi}{k\hat{n}GA} \quad (A.4)$$

$$K_{14} = \frac{\varphi\cos^2\theta\sin^3\theta}{EA} - \frac{\sin\theta r^2\varphi}{EI} + \frac{\sin\theta r^2\varphi}{GP} \quad (A.5)$$

$$K_{15} = \frac{\sin^4\theta\cos\theta\cos\varphi}{EA} - \frac{\sin^2\theta\cos\varphi r^2}{\cos\theta EI} - \frac{\cos\theta r^2\sin\varphi}{GP} \quad (A.6)$$

$$K_{16} = -\frac{\sin^4\theta\cos\theta\sin\varphi}{EA} + \frac{\sin^2\theta\cos\varphi r^2}{\cos\theta EI} + \frac{\cos\theta r^2\sin\varphi}{GP} \quad (A.7)$$

$$k_{21} = \frac{r\sin^3\theta(\cos\varphi - \cos^2\theta\cos\varphi - \sin^2\theta + \sin^2(2\theta))}{EA} + \frac{r^3\sin^3\theta(\sin^2\varphi - \sin\theta + \sin^2(2\theta))}{\cos^2\theta EI} + \frac{r^3\sin\theta\sin(\varphi - \theta)}{GP} + \frac{\sin\theta r\cos\varphi}{k\hat{s}GA} \quad (A.8)$$

$$k_{22} = \frac{\cos[\varphi]}{\left(\frac{512P^4\pi}{3(p^2 + 4\pi^2r^2)} - \frac{8P^2\pi r^2}{p^2 + 4\pi^2r^2} + \frac{32\pi^3r^2}{p^2 + 4\pi^2r^2} + \frac{32\pi^3r^2}{AEP^2 + 4AE\pi^2r^2} + \frac{P^4}{p^2\pi + 4\pi^2r^2} + \frac{8\pi k\hat{s}}{AG} \right)} \left(\frac{8P^2\pi k\hat{n}}{AGP^2 + 4AG\pi^2r^2} - \frac{32P^3\pi M_o}{p^2 + 4\pi^2r^2} - \frac{64P^3\pi x_o}{p^2 + 4\pi^2r^2} - \frac{8P^2\pi M_o x_o}{p^2 + 4\pi^2r^2} + \frac{8P^2\pi x_o^2}{p^2 + 4\pi^2r^2} + 4\pi r^2(15P^2 + 512P^2\pi^2 + 192P\pi^2x_o + 24\pi^2x_o^2 - 24\pi^2M_o(4P + x_o)) \right) \left(3GJ(p^2 + 4\pi^2r^2) + \frac{1}{96\pi^2} \left(\begin{aligned} &4P^2\theta^2 - 6P^2\theta\cos[2\theta] + 3P^2\sin[2\theta] - 6P^2\theta^2\sin[2\theta] + 24P\pi\theta^2x_o - \\ &12P\pi\cos[2\theta]x_o - 24P\pi\theta\sin[2\theta]x_o + 48\pi^2\theta x_o^2 - 24\pi^2\sin[2\theta]x_o^2 + \\ &P\sin[2\theta] + 4\pi\cos[2\theta]x_o + 6\pi M_o \left(\frac{-2P\theta^2 + P\cos[2\theta] + 2P\theta\sin[2\theta]}{8\pi\theta x_o + 4\pi\sin[2\theta]x_o} \right) \end{aligned} \right) \right) \quad (A.9)$$

$$\begin{aligned}
k_{23} = & \frac{\text{Cos}\theta r}{4EA} \left(2\text{Sin}^4\theta \text{Cos}\varphi \text{Sin}\varphi - 2\text{Cos}^2\varphi - 2\text{Cos}^4\theta \text{Cos}^2\varphi \right) + 2\text{Sin}^4\theta \varphi^2 \text{Cos}^2\varphi + 4\text{Cos}^2\theta \text{Cos}^2\varphi - \\
& 4\text{Sin}^4\theta \varphi \text{Cos}^2\varphi - 2\text{Sin}^4\theta \varphi \text{Cos}\varphi \text{Sin}\varphi - \text{Sin}^4\theta \varphi^2 - 4\text{Cos}^2\theta \text{Sin}^2\varphi - 4\text{Sin}^4\theta \varphi \text{Cos}^2\varphi + \frac{r^3}{4\text{Cos}^3\theta \text{EJ}} \\
& \left(\frac{2\text{Sin}^4\theta \varphi^2 \text{Cos}^2\varphi - 2\text{Cos}^4\theta \text{Cos}^2\varphi - \text{Cos}^2\theta \text{Sin}^2\varphi}{2\text{Cos}^4\theta \text{Cos}^2\varphi - \text{Cos}^2\theta \text{Sin}^2\varphi} \right) + \frac{r^3 \text{Sin}^2\theta}{\text{GPCos}\theta} - \frac{\text{Sin}^2\varphi}{k\hat{n}} + \frac{r \text{Cos}^2\varphi \text{Cos}\theta}{2k\hat{s}GA} - \frac{r^3 \text{Sin}^2\theta}{4\text{Cos}^3\theta \text{EI}} \left(2\varphi^2 \text{Cos}^2\varphi - 2\varphi \text{Cos}\varphi \text{Sin}\varphi - \text{Sin}^2\varphi \right)
\end{aligned} \tag{A.10}$$

$$\begin{aligned}
K_{24} = & - \frac{\text{Cos}^3\theta \left(\text{Cos}\varphi - \text{Cos}^2\theta \text{Cos}\varphi - \text{Sin}^2\theta \text{Sin}[2\theta] + \text{Sin}^2\varphi \right)}{EA} - \\
& \frac{r^2 \left(\text{Sin}^2\theta \text{Sin}\varphi - \text{Cos}^2\theta \text{Cos}\varphi - \text{Sin}^2\theta \text{Sin}[2\theta] - \text{Sin}^2\theta \text{Cos}\varphi \right)}{\text{EICos}\theta} + \frac{\text{Sin}^2\theta \text{Sin}\varphi r^2 (\varphi - \theta)}{\text{GPCos}\theta}
\end{aligned} \tag{A.11}$$

$$\begin{aligned}
K_{25} = & - \frac{\text{Cos}^2\theta \text{Sin}\theta}{4EA} \left(2\text{Sin}^2\theta \text{Cos}^2\varphi + 2\text{Cos}^2\theta \text{Cos}\varphi \text{Sin}\varphi - 2\text{Cos}^2\theta - 2\text{Sin}^2\theta \text{Cos}^2\varphi + \text{Sin}^2\theta - 2\text{Cos}\varphi \text{Sin}\varphi \right) \\
& - \frac{\text{Sin}\theta r^2}{4\text{Cos}^2\theta \text{EJ}} \left(\text{Sin}^2\theta \text{Cos}\varphi \text{Sin}\varphi - 2\text{Sin}^2\theta \text{Cos}^2\varphi + 2\varphi \right) - \frac{\text{Sin}\theta r^2 \left(-2\varphi \text{Cos}^2\varphi \right) - \text{Cos}\varphi \text{Sin}\varphi + 3\varphi + 2\varphi \text{Cos}^2\varphi}{4\text{GP}} \\
& + \frac{\text{Sin}\theta r^2 \left(-2\varphi \text{Cos}^2\varphi - \text{Cos}\varphi \text{Sin}\varphi \right)}{4\text{Cos}^2\theta \text{EI}}
\end{aligned} \tag{A.12}$$

$$\begin{aligned}
K_{26} = & \frac{\text{Cos}^2\theta \text{Sin}\theta}{4EA} \left(-2\text{Sin}^2\theta \text{Cos}\varphi \text{Sin}\varphi - \text{Sin}^2\theta + \text{Sin}^2\theta \text{Sin}\theta + 2\text{Sin}^2\theta \text{Cos}\varphi \text{Sin}\varphi - \text{Cos}^2\theta \text{Cos}^2\varphi + \right. \\
& \left. \frac{\text{Sin}\theta r}{\text{Cos}^2\theta \text{EJ}} \left(-2\text{Sin}^2\theta \text{Cos}\varphi \text{Sin}\varphi - \text{Sin}^2\theta + \text{Sin}^2\theta \text{Sin}\theta + 4\text{Gk}\hat{n} \right) + \frac{\text{Sin}\theta r^2 \left(2\varphi\theta - 2\varphi \text{Cos}\varphi \text{Sin}\varphi + \text{Sin}^2\varphi \right)}{4\text{EI}} \right)
\end{aligned} \tag{A.13}$$

$$\begin{aligned}
k_{31} = & \frac{r \text{Sin}^3\theta \left(\text{Cos}^2\theta \text{Sin}\varphi + \text{Sin}^2\theta \text{Cos}(2\theta) + \text{Sin}^2\theta \text{Sin}\varphi - \text{Sin}^2\theta \text{Cos}\varphi \right)}{EA} + \\
& \frac{r^3 \text{Sin}^3\theta \left(\text{Cos}^2\theta \text{Sin}\varphi + \text{Sin}^2(2\theta) \right)}{\text{Cos}^2\theta \text{EI}} + \frac{r^3 \text{Sin}\theta \text{Sin}(\varphi - \theta)}{\text{GP}} - \frac{\text{Sin}\theta r \text{Sin}\varphi}{k\hat{n}GA}
\end{aligned} \tag{A.14}$$

$$\begin{aligned}
k_{32} = & \frac{\text{Cos}\theta r}{4EA} \left(2\text{Sin}^4\theta \text{Cos}\varphi \text{Sin}\varphi - 2\text{Cos}^2\varphi - 2\text{Cos}^4\theta \text{Cos}^2\varphi \right) + 2\text{Sin}^4\theta \varphi^2 \text{Cos}^2\varphi + 4\text{Cos}^2\theta \text{Cos}^2\varphi - \\
& 4\text{Sin}^4\theta \varphi \text{Cos}^2\varphi - 2\text{Sin}^4\theta \varphi \text{Cos}\varphi \text{Sin}\varphi - \text{Sin}^4\theta \varphi^2 - 4\text{Cos}^2\theta \text{Sin}^2\varphi - 4\text{Sin}^4\theta \varphi \text{Cos}^2\varphi + \frac{r^3}{4\text{Cos}^3\theta EJ} \\
& \left(\frac{2\text{Sin}^4\theta \varphi^2 \text{Cos}^2\varphi - 2\text{Cos}^4\theta \text{Cos}^2\varphi}{\text{Cos}^2\theta \text{Sin}^2\theta} \right) + \frac{r^3 \text{Sin}^2\theta}{\text{GPCos}\theta} - \frac{\text{Sin}^2\varphi}{k\hat{n}} + \frac{r \text{Cos}^2\varphi \text{Cos}\theta}{2k\hat{s}GA} - \frac{r^3 \text{Sin}^2\theta}{4\text{Cos}^3\theta EI} \left(2\varphi^2 \text{Cos}^2\varphi - 2\varphi \text{Cos}\varphi \text{Sin}\varphi - \text{Sin}^2\theta \right)
\end{aligned} \tag{A.15}$$

$$k_{33} = \frac{(3AEGJ)(P^2 + 4\pi^2 r^2) \text{Cos}[\varphi]}{8r \left(\frac{6GJP^2 \pi v + 6AEGJP^2 \pi r^2 v + 12AE\pi^4 r^4 v + 24EJ\pi^3 r^2 v k\hat{n} - 12AEGJP\pi^2 r^2 v}{6AE\pi M, (-2GJP\pi r^2 + P^2 + 4GJ\pi^2 r^2)} \right)} \tag{A.16}$$

$$\begin{aligned}
K_{34} = & - \frac{\text{Cos}^3\theta (\text{Cos}^2\theta \text{Sin}\varphi + \text{Sin}^2\theta \text{Cos}[2\varphi] + \text{Sin}^2\theta \text{Sin}\varphi - \text{Sin}^2\theta \text{Cos}[2\varphi] - \text{Sin}\varphi)}{EA} \\
& \frac{r^2 (\text{Cos}^2\theta \text{Sin}\varphi + \text{Sin}^2\theta \text{Cos}[2\theta] - \text{Sin}^2\theta \text{Cos}\varphi)}{EICos\theta} + \frac{\text{Sin}^2\theta r^2 \text{Cos}\varphi(2\varphi)}{\text{GPCos}\theta}
\end{aligned} \tag{A.17}$$

$$\begin{aligned}
K_{35} = & - \frac{\text{Cos}^2\theta \text{Sin}\theta}{4EA} \left(\begin{aligned} & 2\text{Sin}^2\theta \text{Cos}\varphi \text{Sin}\varphi - \text{Sin}^2\theta - \text{Sin}^2\theta \text{Sin}^2\varphi - 2\text{Cos}^2\varphi + 2\text{Cos}^2\theta \text{Cos}^2\varphi - 2\text{Sin}^2\theta \text{Cos}\varphi \text{Sin}\varphi \\ & + 2\text{Sin}^2\theta - \frac{\text{Sin}\theta r^2}{4\text{Cos}^2\theta EJ} (2\text{Sin}^2\theta \text{Cos}\varphi \text{Sin}\varphi - \text{Sin}^2\theta - \text{Sin}^2\theta \text{Sin}^2\varphi - \text{Cos}\varphi \text{Sin}\varphi + 4\text{Cos}^2\varphi) \\ & - \frac{\text{Sin}\theta r^2 (-2\text{Cos}^2\varphi - 2\varphi \text{Cos}\varphi \text{Sin}\varphi + k\hat{n})}{4GP} - 4\text{Cos}^2\theta EI \end{aligned} \right)
\end{aligned} \tag{A.18}$$

$$\begin{aligned}
K_{36} = & \frac{\text{Cos}^2\theta \text{Sin}\theta}{4EA} \left(\begin{aligned} & 2\text{Sin}^2\theta \text{Cos}\varphi \text{Sin}\varphi - \text{Sin}^2\theta - \text{Sin}^2\theta \text{Sin}^2\varphi - 2\text{Cos}^2\varphi + 2\text{Cos}^2\theta \text{Cos}^2\varphi - 2\text{Sin}^2\theta \text{Cos}\varphi \text{Sin}\varphi \\ & + \frac{\varphi \text{Cos}^2\theta \text{Sin}^2\theta}{EA} + 2\text{Sin}^2\theta - \frac{\text{Sin}\theta r^2}{2EJ} (2\text{Sin}^2\theta \text{Cos}\varphi \text{Sin}\varphi - \text{Sin}^2\theta - \text{Sin}^2\theta \text{Sin}^2\varphi - \text{Cos}\varphi \text{Sin}\varphi + 4\text{Cos}^2\varphi) \\ & + \text{Sin}\theta r^2 (-2\text{Cos}^2\varphi - 2\varphi \text{Cos}\varphi \text{Sin}\varphi + k\hat{n}) - \left(\frac{1}{4GP} + \frac{1}{4\text{Cos}^2\theta EI} \right) \end{aligned} \right)
\end{aligned} \tag{A.19}$$

$$K_{41} = \frac{\varphi \cos^2 \theta \sin^3 \theta}{EA} - \frac{\sin \theta r^2 \varphi}{EI} + \frac{\sin \theta r^2 \varphi}{GP} \quad (\text{A.20})$$

$$K_{42} = - \frac{\cos^3 \theta (\cos \varphi - \cos^2 \theta \cos \varphi - \sin^2 \theta \sin [2\theta] + \sin^2 \theta)}{EA} - \frac{r^2 (\sin^2 \theta \sin \varphi - \cos^2 \theta \cos \varphi - \sin^2 \theta \sin [2\theta] - \sin^2 \theta \cos \varphi)}{E \cos \theta} + \frac{\sin^2 \theta \sin \varphi r^2 (\varphi - \theta)}{G P \cos \theta} \quad (\text{A.21})$$

$$K_{43} = - \frac{\cos^3 \theta (\cos^2 \theta \sin \varphi + \sin^2 \theta \cos [2\varphi] + \sin^2 \theta \sin \varphi - \sin^2 \theta \cos [2\varphi] - \sin \varphi)}{EA} - \frac{r^2 (\cos^2 \theta \sin \varphi + \sin^2 \theta \cos [2\theta] - \sin^2 \theta \cos \varphi)}{E \cos \theta} + \frac{\sin^2 \theta r^2 \cos \varphi (2\varphi)}{G P \cos \theta} \quad (\text{A.22})$$

$$K_{44} = \frac{\cos [\varphi]}{r \left(\frac{32LP^3\pi}{P^2 + 4\pi^2 r^2} + \frac{8P^2\pi M_L}{P^2 + 4\pi^2 r^2} - \frac{8LP^2\pi x_o}{P^2 + 4\pi^2 r^2} + \frac{32\pi^3 r^2 (M_L + L(4P + x_o))}{GJ(P^2 + 4\pi^2 r^2)} + \frac{1}{16\pi} \right) (4\pi(2\theta + \sin[2\theta])M_L + L(P(2\theta^2 + \cos[2\theta]) + 2\theta \sin[2\theta] + 4\pi(2\theta + \sin[2\theta])x_o))} \quad (\text{A.23})$$

$$K_{45} = \frac{\sin \theta \cos^4 \theta \cos \varphi}{rEA} + \frac{\sin \theta r \cos \varphi}{EI} - \frac{\sin \theta r \cos \varphi}{G P k \hat{s}} \quad (\text{A.24})$$

$$K_{46} = - \frac{\sin \theta \cos^4 \theta \cos \varphi}{rEA} - \frac{\sin \theta r \cos \varphi}{EI} + \frac{\sin \theta r \cos \varphi}{G P k \hat{n}} \quad (\text{A.25})$$

$$K_{51} = \frac{\sin^4 \theta \cos \theta \cos \varphi}{EA} - \frac{\sin^2 \theta \cos \varphi r^2}{\cos \theta EI} - \frac{\cos \theta r^2 \sin \varphi}{GP} \quad (\text{A.26})$$

$$\begin{aligned}
K_{52} = & -\frac{\text{Cos}^2\theta\text{Sin}\theta}{4EA} \left(2\text{Sin}^2\theta\text{Cos}^2\varphi + 2\text{Cos}^2\theta\text{Cos}\varphi\text{Sin}\varphi - 2\text{Cos}^2\theta - 2\text{Sin}^2\theta\text{Cos}^2\varphi + \text{Sin}^2\theta - 2\text{Cos}\varphi\text{Sin}\varphi \right) \\
& - \frac{\text{Sin}\theta r^2}{4\text{Cos}^2\theta\text{EJ}} \left(\text{Sin}^2\theta\text{Cos}\varphi\text{Sin}\varphi - 2\text{Sin}^2\theta\text{Cos}^2\varphi + 2\varphi \right) - \frac{\text{Sin}\theta r^2 \left(-2\varphi\text{Cos}^2\varphi \right) - \text{Cos}\varphi\text{Sin}\varphi + 3\varphi + 2\varphi\text{Cos}^2\varphi}{4\text{GP}} \\
& + \frac{\text{Sin}\theta r^2 \left(-2\varphi\text{Cos}^2\varphi - \text{Cos}\varphi\text{Sin}\varphi \right)}{4\text{Cos}^2\theta\text{EI}}
\end{aligned} \tag{A.27}$$

$$K_{53} = -\frac{\text{Cos}^2\theta\text{Sin}\theta}{4EA} \left(\begin{aligned} & 2\text{Sin}^2\theta\text{Cos}\varphi\text{Sin}\varphi - \text{Sin}^2\theta - \text{Sin}^2\theta\text{Sin}^2\varphi - 2\text{Cos}^2\varphi + 2\text{Cos}^2\theta\text{Cos}^2\varphi - 2\text{Sin}^2\theta\text{Cos}\varphi\text{Sin}\varphi \\ & + 2\text{Sin}^2\theta - \frac{\text{Sin}\theta r^2}{4\text{Cos}^2\theta\text{EJ}} \left(2\text{Sin}^2\theta\text{Cos}\varphi\text{Sin}\varphi - \text{Sin}^2\theta - \text{Sin}^2\theta\text{Sin}^2\varphi - \text{Cos}\varphi\text{Sin}\varphi + 4\text{Cos}^2\varphi \right) \\ & - \frac{\text{Sin}\theta r^2 \left(-2\text{Cos}^2\varphi - 2\varphi\text{Cos}\varphi\text{Sin}\varphi + k\hat{n} \right)}{4\text{GP}} - 4\text{Cos}^2\theta\text{EI} \end{aligned} \right) \tag{A.28}$$

$$K_{54} = \frac{\text{Sin}\theta\text{Cos}^4\theta\text{Cos}\varphi}{rEA} + \frac{\text{Sin}\theta r\text{Cos}\varphi}{EI} - \frac{\text{Sin}\theta r\text{Cos}\varphi}{\text{GP}k\hat{s}} \tag{A.29}$$

$$K_{55} = \frac{\text{Cos}[\varphi]}{\left(r \left(\begin{aligned} & \frac{32\text{HP}^2\pi}{\text{P}^2 + 4\pi^2r^2} + \frac{8\text{P}^2\pi\text{M}_o}{\text{P}^2 + 4\pi^2r^2} - \frac{8\text{HP}^2\pi\text{x}_o}{\text{P}^2 + 4\pi^2r^2} + \frac{32\pi^3r^2(\text{M}_o - \text{H}(4\text{P} + \text{x}_o))}{\text{GJ}(\text{P}^2 + 4\pi^2r^2)} + \frac{1}{16\pi} \\ & - 4\pi(-2\theta + \text{Sin}[2\theta])\text{M}_o + \text{H}(\text{P}(-2\theta^2 + \text{Cos}[2\theta]) + 2\theta\text{Sin}[2\theta] + 4\pi(-2\theta + \text{Sin}[2\theta] + \text{Sin}[2\theta])\text{x}_o) \end{aligned} \right) \right)} \tag{A.30}$$

$$K_{56} = -\frac{\text{Sin}^2\theta\text{Cos}^3\theta\text{Cos}^2\varphi}{2rEA} - \frac{\text{Sin}^2\theta r\text{Cos}^2\varphi r}{2\text{Cos}\theta\text{EJ}} - \frac{\text{Cos}\theta\text{Cos}^2\varphi r}{2\text{GP}} + \frac{\text{Cos}^2\varphi r}{2\text{Cos}\theta\text{EI}} \tag{A.31}$$

$$K_{61} = -\frac{\text{Sin}^4\theta\text{Cos}\theta\text{Sin}\varphi}{EA} + \frac{\text{Sin}^2\theta\text{Cos}\varphi r^2}{\text{Cos}\theta\text{EI}} + \frac{\text{Cos}\theta r^2\text{Sin}\varphi}{\text{GP}} \tag{A.32}$$

$$K_{62} = \frac{\text{Cos}^2\theta\text{Sin}\theta}{4EA} \left(-2\text{Sin}^2\theta\text{Cos}\varphi\text{Sin}\varphi - \text{Sin}^2\theta + \text{Sin}^2\theta\text{Sin}\theta + 2\text{Sin}^2\theta\text{Cos}\varphi\text{Sin}\varphi - \text{Cos}^2\theta\text{Cos}^2\theta + \right. \\ \left. \frac{\text{Sin}\theta r}{\text{Cos}^2\theta\text{EJ}} \left(-2\text{Sin}^2\theta\text{Cos}\varphi\text{Sin}\varphi - \text{Sin}^2\theta + \text{Sin}^2\theta\text{Sin}\theta + 4\text{Gk}\hat{n} \right) + \frac{\text{Sin}\theta r^2 \left(2\varphi\theta - 2\varphi\text{Cos}\varphi\text{Sin}\varphi + \text{Sin}^2\varphi \right)}{4\text{EI}} \right) \tag{A.33}$$

$$K_{63} = \frac{\cos^2 \theta \sin \theta}{4EA} \left(\begin{aligned} & 2\sin^2 \theta \cos \varphi \sin \rho - \sin^2 \theta - \sin^2 \theta \sin^2 \varphi - 2\cos^2 \varphi + 2\cos^2 \theta \cos^2 \varphi - 2\sin^2 \theta \cos \varphi \sin \rho \\ & + \frac{\varphi \cos^2 \theta \sin^3 \theta}{EA} + 2\sin^2 \theta - \frac{\sin \theta r^2}{2EJ} (2\sin^2 \theta \cos \varphi \sin \rho - \sin^2 \theta - \sin^2 \theta \sin^2 \varphi - \cos \varphi \sin \rho + 4\cos^2 \varphi) \\ & + \sin \theta r^2 (-2\cos^2 \varphi - 2\varphi \cos \varphi \sin \rho + k\hat{n}) - \left(\frac{1}{4GP} + \frac{1}{4\cos^2 \theta EI} \right) \end{aligned} \right) \quad (A.34)$$

$$K_{64} = -\frac{\sin \theta \cos^4 \theta \cos \varphi}{rEA} - \frac{\sin \theta r \cos \varphi}{EI} + \frac{\sin \theta r \cos \varphi}{GPK \hat{n}} \quad (A.35)$$

$$K_{65} = -\frac{\sin^3 \theta \cos^3 \theta \cos^2 \varphi}{2rEA} - \frac{\sin^2 \theta r \cos^2 \varphi r}{2\cos \theta EJ} - \frac{\cos \theta \cos^2 \varphi r}{2GP} + \frac{\cos^2 \varphi r}{2\cos \theta EI} \quad (A.36)$$

$$K_{66} = \frac{GJ (p^2 + 4\pi^2 r^2) \cos [\varphi]}{16 \pi r (-Pr (L(P + GJP) + 2GJ \pi r v) + (p^2 + 4GJ \pi^2 r^2) M_v)} \quad (A.37)$$

Appendix B. Mode shapes (I-DEAS)

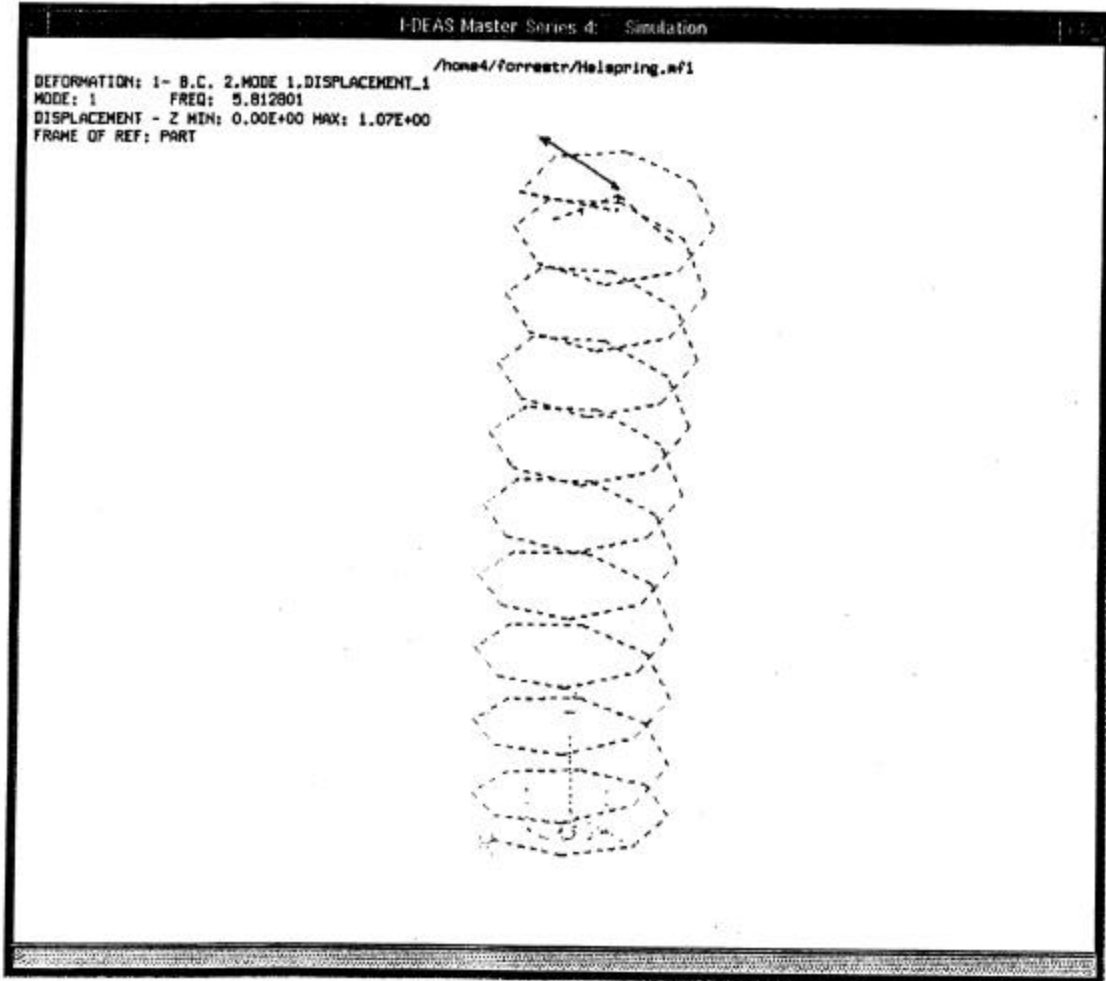


Figure B.1 Y-translation

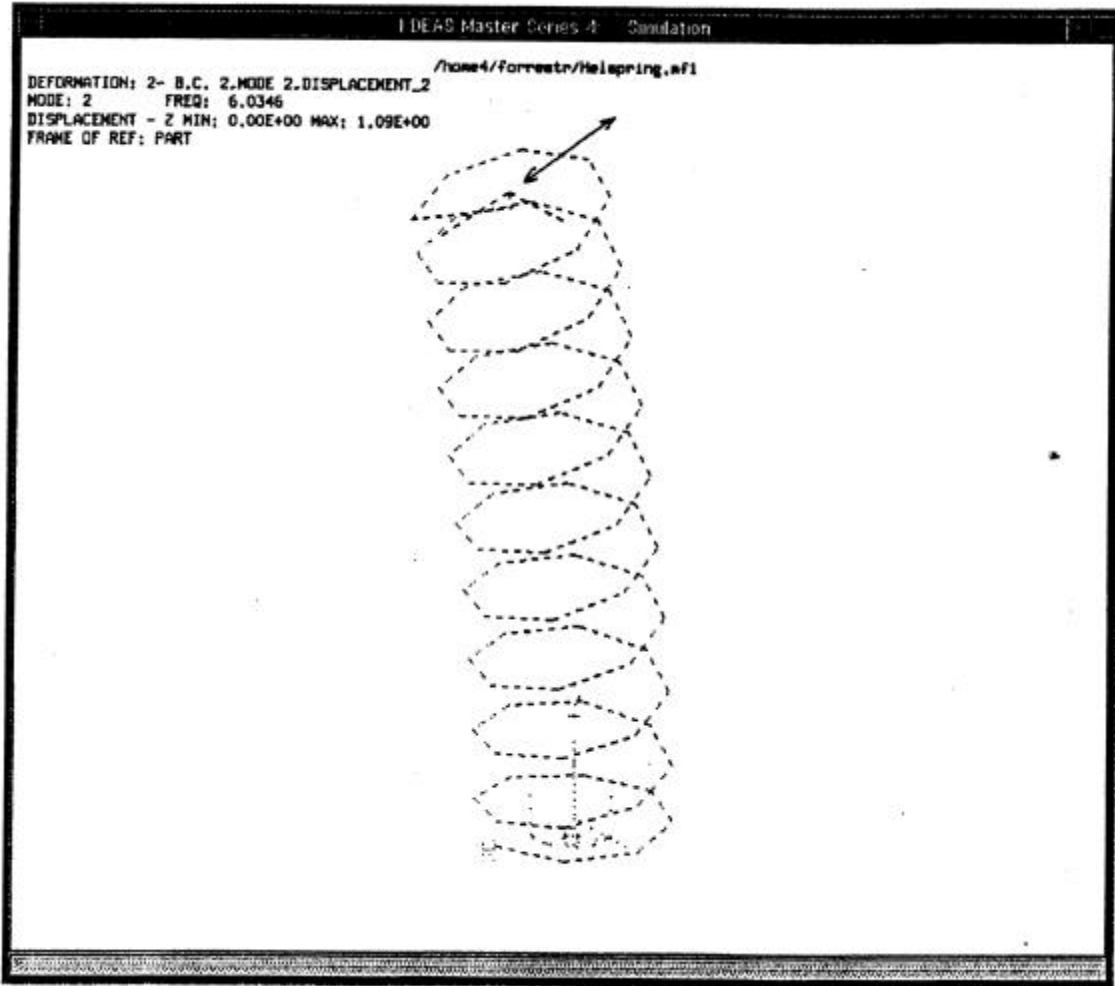


Figure B.2 X-translation

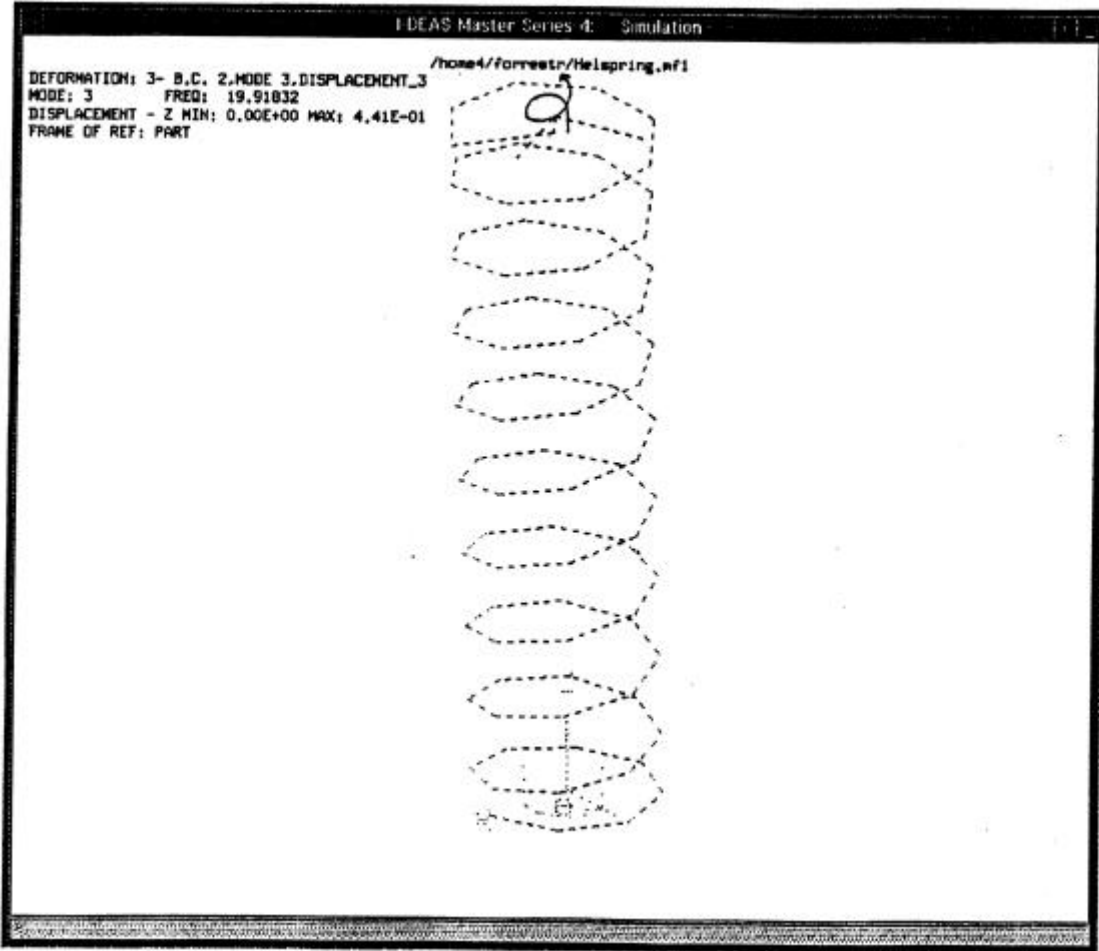


Figure B.3 Z-bending

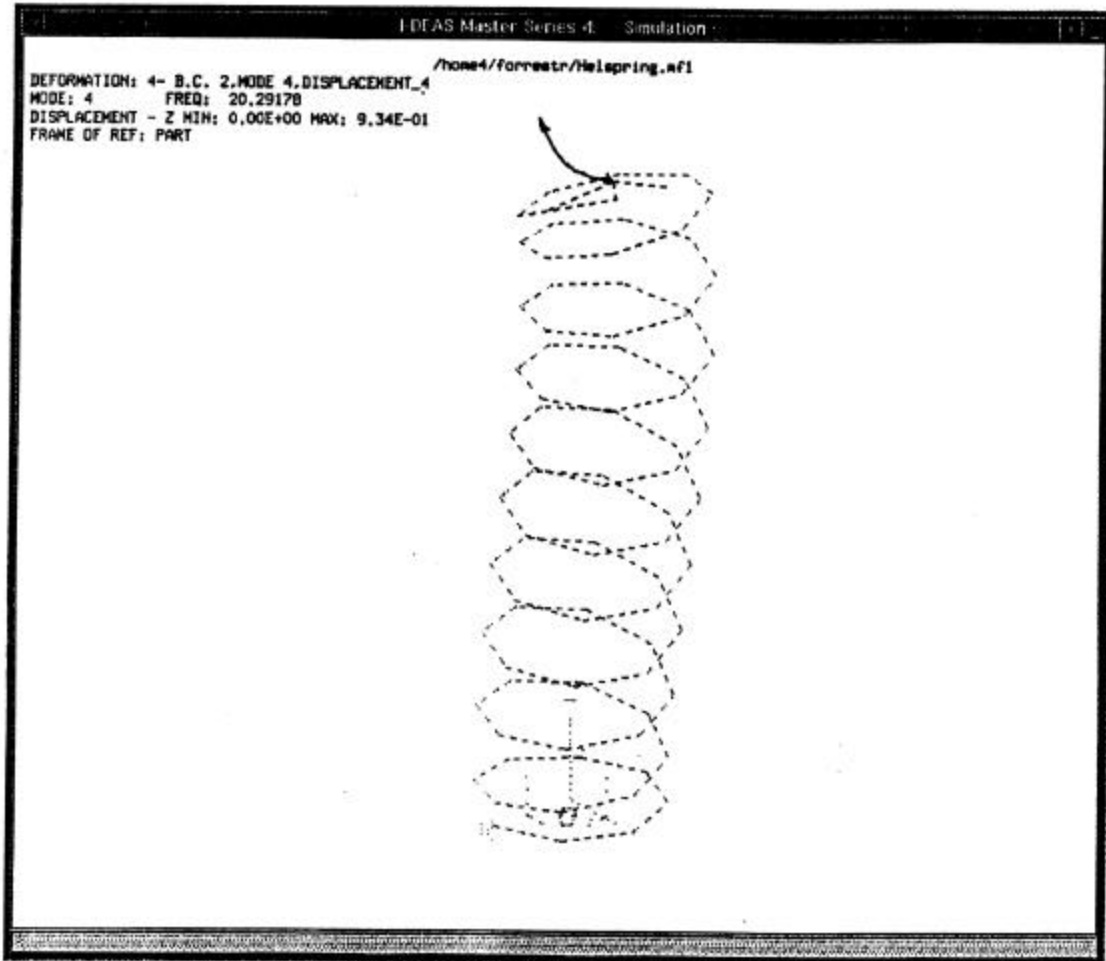


Figure B.4 Y-bending

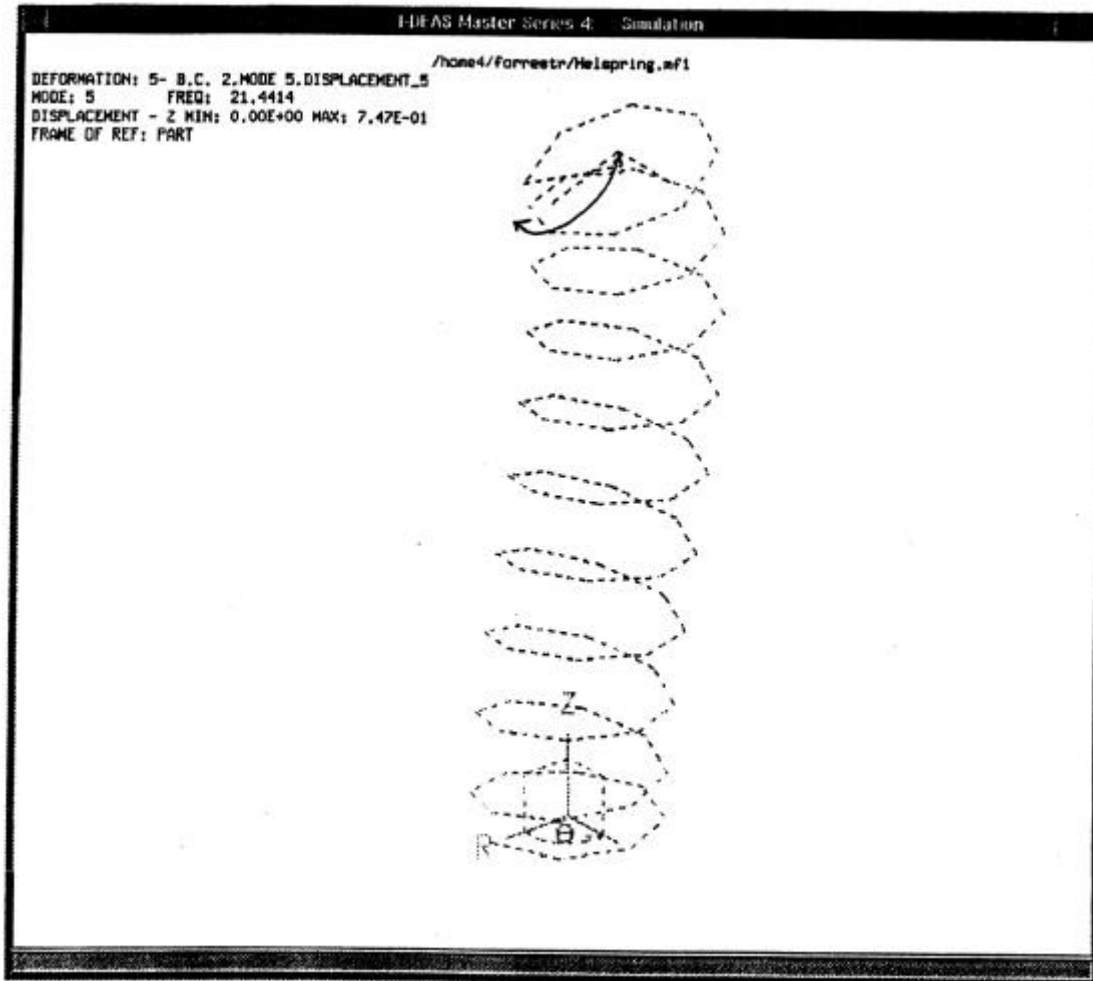


Figure B.5 X-bending

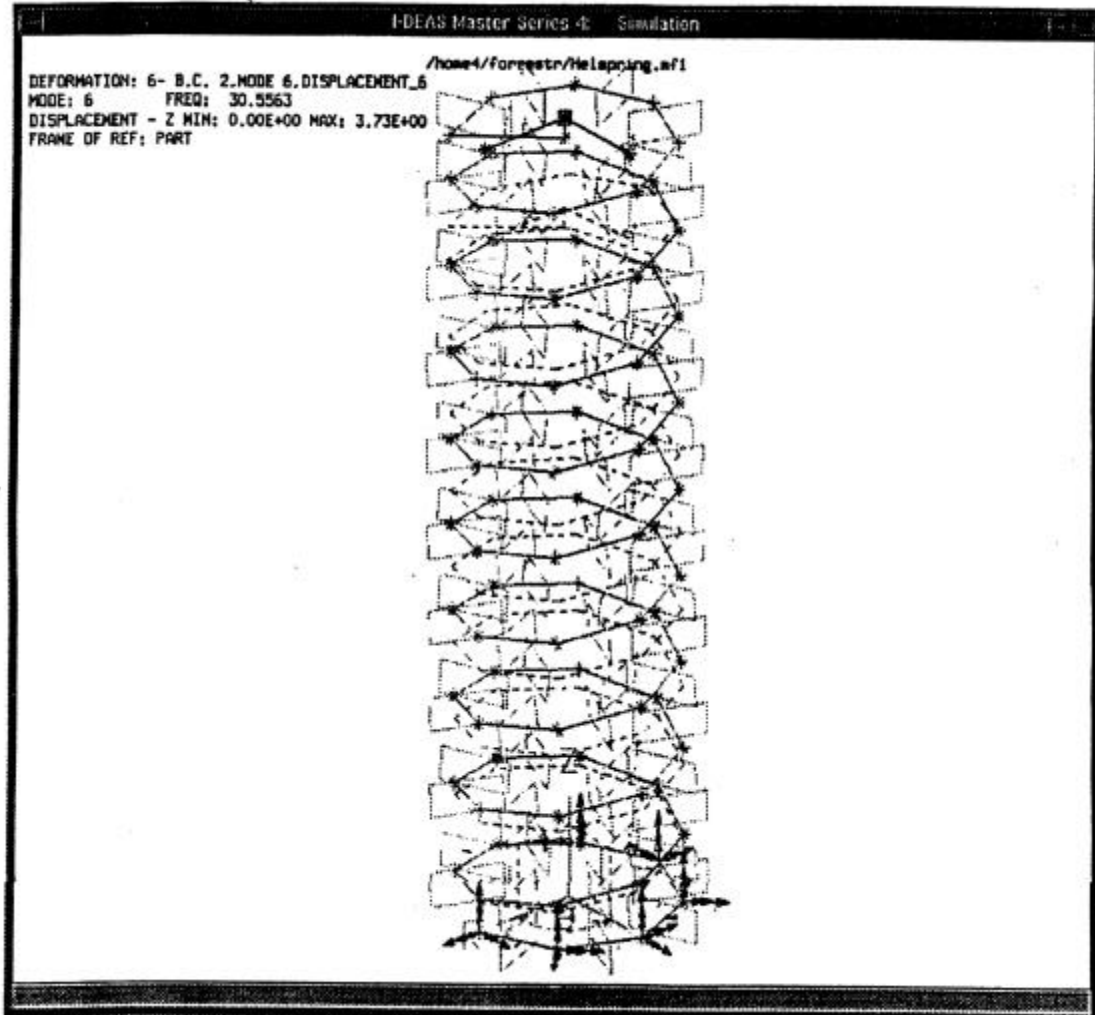


Figure B.6 Z-translation

References

1. Wahl, A.M., "Mechanical Springs", 2nd Edition, McGraw-Hill, Inc. New York, 1978.
2. Haringx, J. A.. "On Highly Compressible Helical springs and Rubber rods, and their application for Vibration-Free Mountings", Parts 1 and 2, Philips Research Reports, Vol. 3: 401-449 and 4:49-80, 1949 (two papers)
3. Biezeno, C. B. and Grammel, R., Technische Dynamik. Berlin, Germany: Verlag.von Julins Springer, 1939. (In Germany): Translated by Oliver Popp
4. Lindkvist, L. "Three-dimensional load -Deformation Relationships of Arbitrarily loaded coiled springs", Machine and Vehicle Design, Chalmers University of Technology, Sweden, 1995.
5. Cook, R.D., Young, W.C., "Advanced Mechanics of Materials", Macmillan Publishing Company, New York 1985.
6. Belingardi, G.I, "Über die seitliche Ausbiegung von zylindrischen schraubendruckfedern", Draht 3, 1988, pp 1101-1103.
7. Thomson, W.T., "Theory of Vibration with Applications", 4th Edition, Printice Hall, Englewood Cliffs, New Jersey, 1993.
8. Langhaar, H.L., "Energy Methods in applied Mechanics", John Wiley and sons, Inc. New York, 1962.
9. Arcot, R.P., "Computer Simulation of the Bristol Compressor Suspension system Dynamics", Department of Mechanical Engineering, Virginia Polytechnic Institute & State University, November 1993.
10. Ramani, A. "Finite Element modeling of an airconditioning compressor for noise prediction applications", Department of Mechanical Engineering, Virginia Polytechnic Institute & State University, December 1993.
11. Richards, T.H, "Energy methods in Stress Analysis", John Wiley and Sons, Inc. New York, 1977.
12. Lawry, M.H., "I-DEAS Master Series™ 2.0, Student Guide, Structural Dynamics Research Corporation, 1994.
13. Cook, R. D., "Finite Element Modeling for Stress Analysis", John Wiley and sons, Inc., 1995.
14. Ewins, D. J., "Modal Testing: Theory and Practice", John Wiley and sons, Inc. New York, 1985.
15. Shigley, J.E., Mischke C.R., "Mechanical Engineering Design", 5th Edition, McGraw Hill Inc., New York 1989.

Vita

Merville K. Forrester was born on April 29th, 1972 in Scarborough, Tobago, W.I. He was raised in Plymouth and completed high school there in 1988. In December 1994, he received his B.S. degree in Mechanical Engineering from Tennessee State University, Nashville, Tennessee. In January 1995, Mr. Forrester enrolled in the College of Engineering at Virginia Polytechnic Institute & State University in Blacksburg, Virginia to pursue a Master of Science degree in Mechanical Engineering.